
DC3DCD: UNSUPERVISED LEARNING FOR MULTICLASS 3D POINT CLOUD CHANGE DETECTION

A PREPRINT

Iris de Gélis^{1,2*}, Sébastien Lefèvre², and Thomas Corpetti³

¹Magellium, Toulouse, France

²IRISA, UMR 6074, Université Bretagne Sud, Vannes, France

³CNRS, LETG, UMR 6554, Rennes, France

ABSTRACT

In a constant evolving world, change detection is of prime importance to keep updated maps. To better sense areas with complex geometry (urban areas in particular), considering 3D data appears to be an interesting alternative to classical 2D images. In this context, 3D point clouds (PCs), whether obtained through LiDAR or photogrammetric techniques, provide valuable information. While recent studies showed the considerable benefit of using deep learning-based methods to detect and characterize changes into raw 3D PCs, these studies rely on large annotated training data to obtain accurate results. The collection of these annotations are tricky and time-consuming. The availability of unsupervised or weakly supervised approaches is then of prime interest. In this paper, we propose an unsupervised method, called DeepCluster 3D Change Detection (DC3DCD), to detect and categorize multiclass changes at point level. We classify our approach in the unsupervised family given the fact that we extract in a completely unsupervised way a number of clusters associated with potential changes. Let us precise that in the end of the process, the user has only to assign a label to each of these clusters to derive the final change map. Our method builds upon the DeepCluster approach, originally designed for image classification, to handle complex raw 3D PCs and perform change segmentation task. An assessment of the method on both simulated and real public dataset is provided. The proposed method allows to outperform fully-supervised traditional machine learning algorithm and to be competitive with fully-supervised deep learning networks applied on rasterization of 3D PCs with a mean of IoU over classes of change of 57.06% and 66.69% for the simulated and the real datasets, respectively. The code is available at <https://github.com/IdeGelis/torch-points3d-DC3DCD>.

Keywords 3D point clouds · Change detection · Unsupervised Deep learning · Deep clustering

1 Introduction

While urban environments are continuously and rapidly evolving, change detection between several temporal acquisitions is a way to quickly highlight modified areas in order to update maps [Demir et al., 2012] or to identify damaged objects [Dong and Shan, 2013] in case of natural disasters. With regard to the complexity of urban landscapes, sensing the area using also vertical information appears to be judicious. Indeed, such three-dimensional (3D) information allows to better characterize environment geometry and to avoid two-dimensional (2D) image problems such as the difference of viewing angles between distinct acquisitions, spectral variability of objects over time, perspective, and distortion effects [Qin et al., 2016]. 3D data are acquired thanks to Light Detection And Ranging (LiDAR) sensor or photogrammetric process, both resulting in 3D Point Clouds (PCs). No matter the type of acquisition, multi-temporal 3D data are generalizing. Indeed, more and more national mapping agencies opt for full territory Aerial Laser Scanning (ALS) campaign, as in the Netherlands with Actueel Hoogtebestand Nederland (AHN) multi-temporal campaigns [Sande et al., 2010], or in France with the LiDAR high density (HD) project whose objective is to propose a complete 3D high resolution coverage of France with regular updates in the future. In the same time satellites mission for 3D

*iris.de-gelis@irisa.fr

sensing are multiplying, e.g., Pléiades [Bernard et al., 2012], Pléiades Néo [Jérôme, 2019], 3D Optical Constellation (CO3D) [Lebègue et al., 2020] missions. In civil engineering, Terrestrial Laser Scanning (TLS) or unmanned aerial vehicle (UAV) photogrammetry are becoming unavoidable for an accurate sense of complex objects. Thereby, this calls for methods able to analyze these multi-temporal 3D data.

Whether related to urban environment [Stilla and Xu, 2023] or geosciences [Okyay et al., 2019], many studies have been focused on handling 3D data for accurate change extraction. Recently, some methods based on deep learning proved their efficiency over traditional distance-based methods and machine learning. While the first deep learning methods for 3D change detection were based on 2.5D rasterization of PCs into Digital Surface Model (DSM) [Zhang et al., 2018a, 2019] or range image [Nagy et al., 2021], most recent works are dealing directly with the raw 3D data. Indeed, although easing the computation, any rasterization process implies a significant loss of information for instance on building facades but also due to aggregation of several points in a cell. Ku et al. [2021] propose to represent PCs by graphs and apply graph convolution operator (EdgeConv) [Wang et al., 2019] to extract discriminative features. However, their proposed method, called Siamese Graph Convolutional Network (SiamGCN), results only in change detection at the scene level, i.e., solving a change classification task. On the opposite, de Gélis et al. [2023a] proposed a network to solve change segmentation task, i.e., providing multiclass change information at point level (so coarser results than change classification). To handle raw 3D PCs, they rely on Kernel Point Convolution (KPCConv) [Thomas et al., 2019]. Their network, named Siamese KPCConv enables to outperform other machine learning methods or DSM-based deep learning methods. More recently, a study [de Gélis et al., 2023b] suggests improving Siamese KPCConv by making the network focusing more on change-related features. To do so, de Gélis et al. [2023b] proposes to provide a hand-crafted feature related to change as input to Siamese KPCConv along with 3D point coordinates. They also developed three other architectures for this particular task. OneConvFusion and Triplet KPCConv contain specific change-related encoder that takes as input only feature difference. Encoder Fusion SiamKPCConv (EFSKPCConv) concatenates both change and mono-date information directly in the encoder. This latter achieves the best results compared to previous state-of-the-art methods.

Although efficient, these deep learning-based methods are supervised, i.e., require large databases for the training of the network. For change segmentation, millions of points should be annotated according to the change type. This annotation is often performed manually because any automatization process is not obvious due to PCs characteristics such as the lack of point-to-point matching, sparsity, or occlusions (see the example of AHN Change Detection (AHN-CD) dataset [de Gélis et al., 2023a]). Therefore, it is important to develop methods that require none or at least less annotations to perform 3D change segmentation. As stated in recent surveys [Kharroubi et al., 2022, Xiao et al., 2023], the literature still lacks of methods for unsupervised or weakly supervised learning when dealing with 3D PCs change detection. Indeed, nowadays unsupervised methods are mostly traditional rule-based methods that are often very specific to a dataset. Also, recently an adaptation of Deep Change Vector Analysis (DCVA) [Saha et al., 2019] to 3D PCs change detection has been proposed based on self-supervised learning [de Gélis et al., 2023c]. However, this unsupervised method only deals with binary change segmentation, thus the method is not able to distinguish between multiple classes of changes. Thereby, in this paper, we propose an unsupervised learning strategy to deal with multiclass 3D PCs change segmentation. The strategy is based on deep clustering principle and in particular on DeepCluster [Caron et al., 2018]. Deep clustering consists in jointly optimizing deep representation of the data and performing clustering with learned features [Ren et al., 2022, Zhou et al., 2022]. This strategy has received increasing interest for 2D image unsupervised representation learning in computer vision [Caron et al., 2018, Cho et al., 2021]. However, as far as the change detection task is concerned, the use of deep clustering is less common. Zhang et al. [2018b] and Dong et al. [2021] propose to rely on an unsupervised clustering of deep feature representations to further train their network to perform change detection. In Zhang et al. [2018b] a stack of fully-connected layers is used to learn Gaussian-distributed and discriminative difference representations for non-change and different types of changes. Dong et al. [2021] further improves the latter by using a Convolutional Neural Network (CNN) relying on multi-scale self-attention. Another study partially uses deep clustering principle for 2D binary change detection by introducing a deep clustering loss jointly with contrastive and appealing losses to make a CNN network learning discriminative mono-date features. These features are further compared using DCVA principle to extract binary changes in multi-modal optical and Synthetic Aperture Radar (SAR) images [Saha et al., 2021]. This principle was adapted in de Gélis et al. [2023c] for 3D PCs binary change detection. Finally, to the best of our knowledge, Zhang et al. [2021] is the first study using the deep clustering principle on 3D data. However, the approach relies on a voxelisation of the PC instead of dealing with the raw PC directly, and performs classification at the scene level and not at the point level (a.k.a. segmentation).

The contributions of this work are thus as follows:

1. To the best of our knowledge, we propose the first unsupervised learning strategy for multiclass change segmentation into raw 3D PCs.
2. We build upon DeepCluster [Caron et al., 2018] to tackle the change segmentation task in 3D PCs. To do so, we experiment our model with several 3D PCs change segmentation architectures.

3. After analyzing the learning behavior, we evaluate our method on both real and simulated public datasets, and provide comparisons with supervised, unsupervised and weakly-supervised methods.
4. We demonstrate that our model, if provided with a perfect binary change map, can compete with fully supervised deep methods for multiclass change segmentation.

The description of our method is given in Section 2. The results are provided in Section 3 and discussed in Section 4. Finally, the conclusion is provided in Section 5. The implementation of our method will be made available at [link](#)².

2 Unsupervised 3D change detection

We describe here our 2-step methodology to compare two 3D PCs and classify the second one with several types of changes. Since our study does not focus on PCs registration, we assume that the PCs have been already registered. Various registration techniques exist and one can use for instance the Iterative Closest Point algorithm [Besl and McKay, 1992]. The first step, called DC3DCD, is fully unsupervised and does not need any labeling of the PCs. It relies on the concept of deep clustering, that is first recalled in Sec. 2.1. We then explain how deep clustering can be used to solve the 3D PC change detection problem in Sec. 2.2, where we detail the backbone model, the use of a prototype layer, the input data needed to feed the network, and some specific elements of the training procedure. This fully unsupervised step based on DC3DCD leads to a clustering of the PCs into different clusters or pseudo-labels. A second step is then required to map these pseudo-labels into real labels. Only here is the user involved, through a manual mapping process limited to the number of clusters (and not the number of points). This weakly-supervised step is detailed in Sec. 2.3.

2.1 DeepCluster principle

Among the variety of studies related to deep clustering [Ren et al., 2022, Zhou et al., 2022], DeepCluster appears to be among the most fundamental ones. Proposed by Caron et al. [2018], this method resides in a rather simple idea of alternatively clustering deep latent representation of data to obtain pseudo-labels further used to train a CNN. In particular, the convolutional network is trained in a supervised manner using pseudo-labels as objective for prediction. In a traditional supervised approach, giving a set of N images x_n ($n \in [1, N]$), a parametrized classifier g_W predicts the correct labels (y_n) using the features extracted by $f_\theta(x_n)$ (W and θ being the parameters from the classifier and the back-bone convolutional model, respectively). They are optimized according to the following problem:

$$\min_{\theta, W} \frac{1}{N} \sum_{n=1}^N \ell(g_W(f_\theta(x_n)), y_n) \quad (1)$$

where ℓ is the loss function, a classical negative log-likelihood (NLL) in their method. This cost function is minimized using standard mini-batch stochastic gradient descent and backpropagation to compute the gradient. The difficulty in an unsupervised setting is therefore to define y_n .

In DeepCluster, Caron et al. [2018] proposed to rely on a classical clustering algorithm such as k -means [MacQueen, 1967] or power iteration clustering (PIC) [Lin and Cohen, 2010] to obtain a pseudo-label (y_{PL_n}) that is used instead of y_n . Caron et al. [2018] showed that the choice of the clustering algorithm is not crucial. Thereby, for illustration purposes, we continue with the example of k -means algorithm. This clustering method matches data to k groups (pseudo-clusters) by minimizing distance between each data and its corresponding cluster center, called centroid (and contained in the centroid matrix C in practice).

Finally, the unsupervised training process alternates between i) clustering the output features of the back-bone convolutional model ($f_\theta(x_n)$) (clustering step), and ii) updating parameters θ and W using the obtained pseudo-labels (y_{PL_n}) thanks to Equation 1 (training step). This relies on the fact that a Multi-Layer Perceptron (MLP) classifier on top of a standard CNN with randomly initialized weights (θ) provides results far above from the chance (i.e., random) level [Noroozi and Favaro, 2016].

In practice, a few tricks are required to prevent trivial solutions, e.g., assigning all the inputs to the same cluster. First, empty clusters are avoided by randomly dividing in two groups the largest cluster when an empty cluster appears. Second, if the pseudo-cluster representation of data is largely imbalanced, the deep model will tend to assign all data to the most represented pseudo-cluster. To counter this, they propose to sample input images during the training based on a uniform distribution over the pseudo-labels.

They showed the robustness of their method by training different architectures (Alexnet [Krizhevsky et al., 2017] and VGG-16 [Simonyan and Zisserman, 2014]) on ImageNet [Deng et al., 2009] or YFCC100M [Thomee et al., 2016] images datasets.

²The code will be made available upon publication.

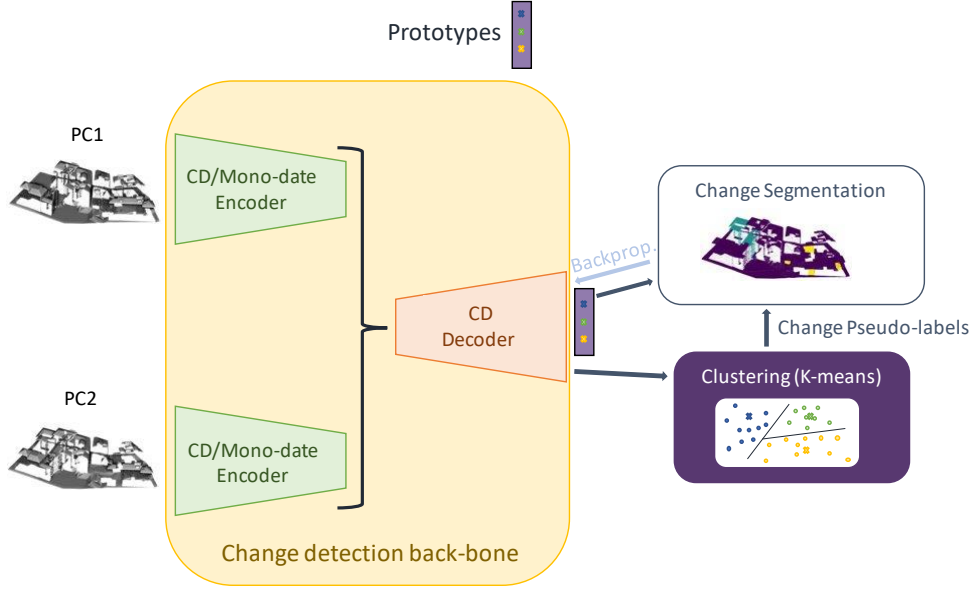


Figure 1: **Illustration of our proposed method: DC3DCD.** It is trained by alternatively clustering deep features to match a pseudo-label to each point of PC 2. These pseudo-labels are used to optimize the back-bone trainable parameters.

In the following, we adapt this principle to 3D PCs change detection.

2.2 DC3DCD: unsupervised learning for 3D multiple change extraction

Whereas the task and the data (2D image classification) of DeepCluster is far from 3D PCs multiple change segmentation, we nevertheless decided to adapt this method to our task and particular data. By replacing the CNN by a 3D PCs change detection back-bone, some change-related features can be extracted. Thereby, the clustering of these deep features results in change-related pseudo-clusters. We further rely on these pseudo-clusters to optimize the trainable parameters θ of the change detection back-bone. Figure 1 illustrates our method called DeepCluster 3D Change Detection (DC3DCD).

Algorithm 1 Fully unsupervised DeepCluster 3DCD training

```

Initialize the back-bone trainable parameters  $\theta$ 
for  $e \leftarrow 1$  to  $\mathcal{E}$  do
  Run mini-batch  $k$ -means to obtain centroids  $C$  on the whole training set
  Assign to each point of the training set a pseudo-cluster
  Replace parameters of the prototype layer by  $C$ 
  Compute the weights  $W_k$  considering pseudo-label distribution in the training set
  Training sample selection: random drawing considering  $W_k$ 
  for  $i \leftarrow 1$  to  $\mathcal{I}$  do
    Use  $\mathcal{L}_{NLL}$  (weighted by  $W_k$ ) to modulate the back-bone trainable parameters ( $\theta$ ) considering pseudo-labels

```

The overall training process of our method is given in the Algorithm 1. Even if the general idea of DeepCluster remains, some specific features of DC3DCD distinguishing it from the original DeepCluster idea should be noted, as described in the following.

2.2.1 Back-bone model

Because of the unstructured nature of 3D PCs, traditional CNN models cannot be applied on them and furthermore, they do not output change-related deep features, but they rather characterize each input independently. To cope these issues, some studies have recently proposed different architectures for supervised change detection in 3D PCs (see section 1). These architectures can therefore be used as a back-bone to our unsupervised method. In practice, both *Siamese KPConv* [de Gélis et al., 2023a] and *Encoder Fusion SiamKPConv* [de Gélis et al., 2023b] will be experimented. *Siamese KPConv* architecture is chosen because it is the first architecture to perform change segmentation into raw 3D

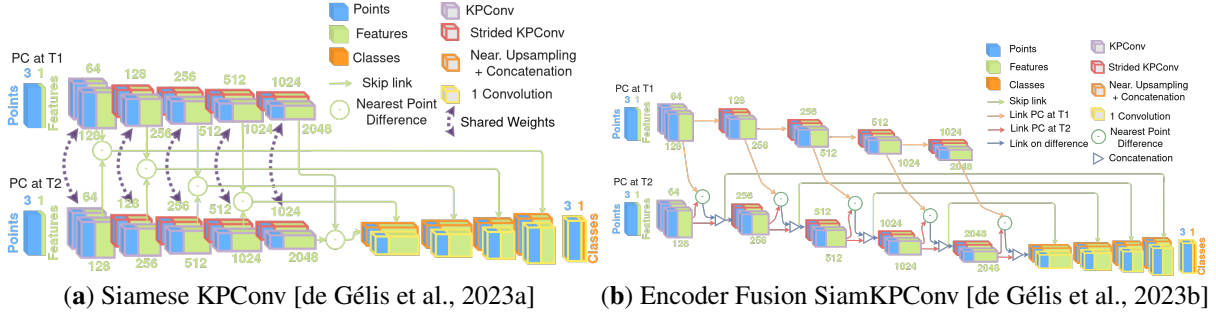


Figure 2: **Back-bone architectures used in our experiments.**

PCs. It extends the idea of Siamese networks with the KPConv convolution principle, as can be seen in Figure 2a. The very recent *Encoder Fusion SiamKPConv* is experimented as well since it has been shown in de Gélis et al. [2023b] that it outperforms other state-of-the-art methods including *Siamese KPConv*. The main idea behind this architecture is no more to encode the two PCs independently (as *Siamese KPConv* do) but rather to include the change information along the encoding process, as can be seen in Figure 2b where the encoding in the bottom part takes into account also the differences between features.

Thus, parameters θ to be optimized are parameters of these back-bone architectures.

2.2.2 Use of a prototype layer

In the original version of DeepCluster, the final classification layer of g_W is re-initialized before each parameter optimization session (i.e., training steps) because there is no matching between two consecutive cluster assignments. A further improved version of DeepCluster (DeepCluster-V2) was proposed by Caron et al. [2020] where the classifier g_W is replaced by the prototypes, i.e., cluster centers. This ends up with an explicit comparison of the features and the centroid matrix C , and tends to improve stability and performance of DeepCluster. According to preliminary experiments, we also decided to use the centroid matrix C defining pseudo-cluster centers. Therefore, the last fully connected layer parameters of the back-bone are set using the centroid matrix C . This so-called prototype layer is updated after each clustering step and fixed during the training step.

2.2.3 Input data

We aim at detecting changes into raw 3D PCs. The back-bone (Siamese KPConv or Encoder Fusion SiamKPConv) is able to compute features directly in 3D PCs. However, given their large size, the PCs cannot be used directly to feed the network, and splitting the input data into smaller subsets is required (similarly to the decomposition of an image into patches in the 2D case). We follow here the strategy we already used in the supervised case [de Gélis et al., 2023a,b] and opt for a decomposition into (pairs of) vertical cylinders, that has been shown to be more relevant than (pairs of) spheres when PCs have a privileged orientation, as for airborne 3D PCs in our settings. Indeed, the changes are more prone to occur in the vertical direction (e.g., new building or demolition), as illustrated in Sec. 3. Please note that our methodology can be easily applied with other neighborhood shapes, such as spheres as already done for supervised cliff erosion monitoring [de Gélis et al., 2022].

Furthermore, in their experimentation, Caron et al. [2018] provides Sobel-filtered images as input to the CNN instead of Red Green Blue (RGB) images. Sobel filtering acts as an edge detector thanks to the computation of gradients on the image. This seems an important step in their method [Caron, 2021, Mustapha et al., 2022] and acts as a pre-computation of relevant features. However, when dealing with 3D PCs, there is no direct equivalent to Sobel filtering. Thus, we rely on some predefined features commonly used to characterize 3D PCs. Let us note that using such features can help the network, as already shown in a supervised scenario [de Gélis et al., 2023b]. As such, we consider here some handcrafted features already used in a Random Forest (RF)-based change detection context [Tran et al., 2018]:

- Point distribution represented by point normals and information on the distribution of points in the neighborhood (i.e., linearity, planarity, and omnivariance).
- Height information characterized by rank of the point on vertical axis in the neighborhood, maximum range of elevation of points in the neighborhood, and normalized height according to the local Digital Terrain Model (DTM) (rasterization of the PC at the ground level).

- Change information described through a feature called stability (ratio of the number of points in the neighborhood of the current PC to the number of points in the neighborhood in the other PC).

We refer the reader to the original paper [Tran et al., 2018] for a detailed description of these features.

2.2.4 Training considerations

Change segmentation task implies assigning a pseudo-label to each point of the second PC (of pairs of the training set). Considering the size of the training set, to fit in memory, a mini-batch k -means [Sculley, 2010] clustering is used. The principle of splitting the largest cluster when an empty cluster appears is used as in DeepCluster.

Change detection datasets are highly imbalanced. To avoid falling in a trivial solution where the back-bone predicts all points with the same label, after each clustering step weights W_k (considering pseudo-labels distribution) are computed. These weights are further used to both select training cylinders and weight the loss (\mathcal{L}_{NLL}). Let us note that this cylinder selection process was also applied in the supervised context [de Gélis et al., 2023a] (on the real labels though). It aims at giving more training samples of underrepresented pseudo-clusters. It also acts as a kind of data augmentation because from one epoch to another, selected cylinders differ according to the random drawing of the cylinder’s central point. Without this trick, the method is likely to collapse to a single class prediction.

During the training step, data augmentation appears to be crucial for stability and performance of the method. In particular, the following data augmentation strategies are used: random cylinders rotation around the vertical axis (same angle for both cylinders of a pair), and addition of a Gaussian noise at point level.

2.3 From predicted pseudo-labels to real labels

The above training using DC3DCD method is fully unsupervised, thereby no use of a ground truth is required. At the end of the overall training process, the back-bone predicts labels for all points of the second PC according to the change. Predicted labels do not directly correspond to the real labels. There is an oversegmentation of PCs induced by the choice of K , the number of pseudo-clusters, which is often large compared to the number of real classes. By opting for such an oversegmentation setting, we expect to be able to address various use cases with different size and precision of classes. One real class is then composed of several predicted clusters, while we assume a predicted cluster to contain only one real class. To map a real label onto each predicted label, a mapping step is necessary. For this mapping, we consider that the user should be involved in order to select the kind of changes that are of interest given the use case. DC3DCD enables to train a back-bone to segment the PC into small areas containing the same types of change or unchanged objects. Thus, the user just has to select for each predicted cluster a corresponding real class. It can be viewed as a kind of active learning process. This is illustrated in Figure 3. This strategy finally involves K annotations to obtain a final change segmentation over the whole testing set (no matter its size). K corresponds to the number of pseudo-clusters used during the training. This hyper-parameter has to be set beforehand. For this reason, our method can be viewed as weakly supervised since K annotations by a user are required in the end of the process. However, these annotations are not taken into account in the learning process, and we therefore classify our approach in the family of unsupervised methods.

Note that although a labelling effort is required for this user-guided mapping, we argue that DC3DCD helps to greatly reduces this effort, as only K annotations are necessary to predict changes throughout the complete dataset. In contrast, conventional deep network training requires annotations for millions of points.

In our experimental settings, we actually do not involve such a manual labelling step but mimic it through an automatic mapping strategy by relying on the ground truth labels provided with the public datasets. More precisely, each pseudo-cluster is assigned a real label by identifying its majority real class. This method seems natural since in a really manual mapping the user typically examines the pseudo-cluster and assigns the most likely label, i.e., the class that corresponds to the majority of points within the pseudo-cluster.

3 Experimental results

In this part, we first present the experimental settings and protocol in Sec. 3.1. Since the proposed approach is unsupervised, a special attention must be given to the learning process, which behaves differently than in a more straightforward supervised situation. Therefore, we also analyze the learning behavior in Sec. 3.2. We finally report our experimental results on both simulated and real data in Sec. 3.3 and 3.4, respectively.

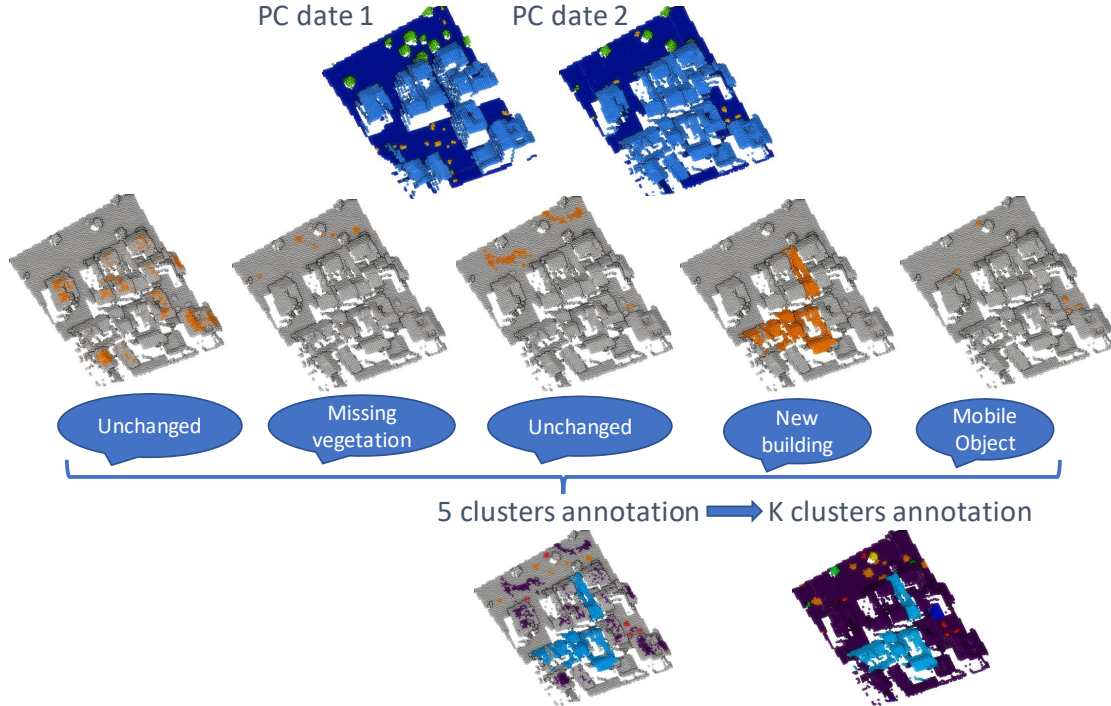


Figure 3: **User guided mapping of predicted clusters to real classes.** For the K predicted clusters, a mapping with the corresponding real class is performed by a user to obtain the final change segmentation of the PC. 5 mappings are provided for the sake of illustration. Segmenting the whole dataset requires K annotations only. This is far less than the millions of points that need to be annotated in order to build training and validation sets in a supervised setting.

3.1 Experimental settings and protocol

We detail here how we set the main hyper-parameters and we describe our experimental settings.

3.1.1 Datasets

Both simulated and real datasets will be experimented, considering Urb3DCD-V2 in low density LiDAR configuration [de Gélis et al., 2021, 2023a] and AHN-CD [de Gélis et al., 2023a]. To the best of our knowledge, these are the only public datasets for change segmentation. The Urban 3D Change Detection (Urb3DCD) dataset is composed of simulated ALS PCs over a french city model (Lyon, France). A simulator is used in order to obtain an accurate annotation of 3D points concerning multiclass changes. Conversely, AHN-CD dataset is made of real ALS PC from AHN campaigns over the Netherland [Sande et al., 2010]. Let us note that the registration of the PCs conducted by the Netherlands AHN services may contain some minor registration errors. The change ground-truth is obtained thanks to a semi-automatic process. In de Gélis et al. [2023a], it has been shown that this process is not perfect since it results in a lot of misclassifications. Therefore, the test set of this dataset will be used for qualitative assessment only. As for quantitative assessment, AHN-CD comes with a manually annotated sub-part of the test set, on which we will report and compare quality scores. Note that during the training, we make no use of the ground truth unless for the method assessment purpose (see Section 3.2). The first sub-sampling rate dl_0 is set to 1 m and the cylinder radius to 50 m for Urb3DCD-V2-1. While for AHN-CD dl_0 is set to 0.5 m and the cylinder radius to 20 m because of the difference of density between both datasets.

3.1.2 Number of pseudo-clusters K

As shown in different studies related to DeepCluster [Caron et al., 2018, Mustapha et al., 2022], choosing the number of pseudo-clusters is important. We experimented several values for K on the simulated dataset and found that $K = 1000$ was an adequate compromise between the stability of the training process and the complexity of the segmentation (i.e., the number of clusters). Indeed, a too small value may not reflect all different types of changes (and thus does not allow

the user to select the changes of interest), while a too large value leads to high training and annotation times. The same value will also be used with the real dataset AHN-CD.

3.1.3 Training step and parameters optimization

For the training process, a Stochastic Gradient Descent (SGD) with momentum of 0.98 is applied to minimize a point-wise NLL loss using the pseudo-labels defined in the clustering step. A batch size of 10 is used. The initial learning rate is set to 10^{-3} and scheduled to decrease exponentially. As in Caron et al. [2018], we experimentally verified that reassigning the clustering after each epoch is better than an update after each n epochs. Indeed, if several training epochs are conducted, the model seems to converge in the first local minimum associated with a non-optimal pseudo-clustering. In each epoch, 3,000 cylinder pairs are seen by the model. A total of 55 epochs, i.e., 55 clustering and training steps, is performed.

3.1.4 Comparisons with supervised methods

A comparison with the only (to our knowledge) existing deep supervised methods is provided, namely *Siamese KPConv* [de Gélis et al., 2023a], *Encoder Fusion SiamKPConv* [de Gélis et al., 2023b], DSM-based deep learning methods (adaptation of Daudt et al. [2018] networks to DSM inspired by Zhang et al. [2019]). Results of a RF algorithm trained on hand-crafted features [Tran et al., 2018] are also given. For all these methods, the full training set available in the dataset (Urb3DCD-V2 or AHN-CD), made of millions of points, is used during the training step. Thus, these methods are expected to outperform our DC3DCD given the vast amount of additional labels they rely on. However, as already stated in the introduction, the literature is still very poor concerning unsupervised methods for change detection in 3D PCs. To the best of our knowledge, there is even no other unsupervised method for 3D PCs multi-class change detection, thus preventing us from conducting fair comparisons.

3.1.5 Adaptation of a supervised method to a weakly supervised setting

To evaluate the benefit of our method, we propose a comparison with deep learning-based supervised methods tuned to a weakly supervised setting. In practice, we use *Encoder Fusion SiamKPConv*, the best of supervised techniques according to de Gélis et al. [2023b]. To this end, we trained it with the same amount of annotated data as our DC3DCD setting. However, this is not straightforward since this network cannot be trained with only 1,000 points. Indeed, as during the supervised training of this network, labels should be provided for each point of the second PC of the pair, and as a cylinder contains more than 1,000 points (about 3,500), we cannot directly compare the supervised training with the same amount of labels (i.e., $K = 1000$). Thus, for both training and validation sets, we chose 7 cylinders, each one centered on one of the 7 classes contained in Urb3DCD-V2 to be sure that each class is represented. Note that with this minimal training configuration, the number of annotated points in the 14 cylinders is around 50,000. As 7 cylinders are less than the batch size of 10 used for all other deep learning-based methods, we also provide results with a batch size of 2.

3.1.6 Comparisons with unsupervised methods

To the best of our knowledge, there is no other weakly supervised or unsupervised deep learning method tackling 3D PCs multiple change segmentation. Thereby, we provide a comparison with a k -means algorithm applied on the ten hand-crafted features of Tran et al. [2018] dedicated to change detection in 3D PCs. Note that LiDAR specific features (e.g., intensity or number of echoes) used in Tran et al. [2018] are ignored here since the simulated dataset does not contain such information. For fair comparison, the k -means is set to predict also $K = 1,000$ pseudo-clusters. The same user-guided mapping is done as proposed in the previous section (Figure 3) to assign the final classes.

While there is no existing unsupervised deep learning method for multiclass change segmentation, the binary case was first and recently tackled in [de Gélis et al., 2023c]. In this setting, only two classes are considered (change and unchanged). In order to compare our method to other unsupervised deep learning models, we have decided to also including a comparison with the methods proposed in [de Gélis et al., 2023c]. They rely on DCVA strategy to highlight binary change information. The deep features used in the comparison are extracted via trained models using a Self-Supervised Learning (SSL) strategy in SSL-DCVA method, or a training on a semantic segmentation task using an available public dataset (namely Hessigheim 3D (H3D) [Kölle et al., 2021]) in SSST-DCVA method. The binary change segmentation experiment is conducted only on the AHN-CD dataset, since the Urb3DCD dataset does not respect some hypothesis required for SSL-DCVA (we refer the reader to the original paper [de Gélis et al., 2023c] for more details).

Before presenting the quantitative results, we analyze in the next section the behavior of the network during the training process.

3.2 Analysis of the learning process

Before presenting the results on the different datasets, we propose to study the behavior of DC3DCD during the training phase. To do so, we rely on the *Encoder Fusion SiamKPConv* back-bone and the configuration without the use of the ten hand-crafted features as input, so considering only 3D points coordinates. Note that the same tendencies are obtained with hand-crafted features or with *Siamese KPConv* back-bone, but we prefer to show results with a network that takes into account the minimum information regarding changes. In practice, we compute criteria associated with the clustering quality and the pseudo-cluster distribution along the training process.

3.2.1 Clustering quality

The evolution of the clustering quality during training epochs is computed by comparing the pseudo-clusters obtained thanks to the k -means on deep features, and the real classes. More precisely, we compute the normalized mutual information (NMI) given by the following formula:

$$\text{NMI}(Y, Y_C) = \frac{I(Y, Y_C)}{\sqrt{H(Y)H(Y_C)}} \quad (2)$$

where Y and Y_C contain the probabilities p_i, p_{C_i} , of each label $i = \{1 \dots N\}$ associated with the true and pseudo-labels. H is the entropy defined as:

$$H(Y) = - \sum_{i=1}^N p_i \log_2 p_i \quad (3)$$

and I is the mutual information, defined as:

$$I(Y, Y_C) = H(Y) - H(Y|Y_C) \quad (4)$$

Intuitively, the NMI is a measure of the information shared between two clusterings, i.e., in our case the clustering of deep features and real classes. If the NMI is equal to 0, the two clusterings are totally independent. On the opposite, if the NMI is equal to 1, there is a perfect correlation between the two clusterings, i.e., one of them is deterministically predictable from the other.

We present the evolution of the clustering quality along the epochs in Figure 4a by giving the NMI between the clustering and the real labels of Urb3DCD-V2 dataset. As can be seen, the clustering tends to get closer to real classes along with the training process. It seems to stabilize after 30-40 epochs. Let us remark that at the end of the training, the NMI is around 0.35. It is still far to 1, but the same trend was observed in DeepCluster training quality assessment by Caron et al. [2018]. In Figure 4b, we evaluate the number of reassignments of cluster from one epoch to the following using the NMI between the clustering of the two epochs. It seems that during the first epochs, there is an important evolution of the clustering, but the training rapidly converges to a rather stable clustering ($NMI > 0.8$). Again, the same tendency was obtained by Caron et al. [2018] for DeepCluster on ImageNet dataset.

3.2.2 Pseudo-cluster distribution

As for the pseudo-cluster distribution, we remind that, ideally, a pseudo-cluster contains only one real class, and a real class can be distributed into several pseudo-clusters. To measure the purity of a pseudo-cluster, we investigate the entropy H (Equation 3) of each pseudo-cluster. If it is near 0, then the pseudo-cluster contains almost only one real class. However, if a pseudo-cluster is divided into several classes, the entropy is higher. In Figure 5 is given the entropy for each pseudo-cluster at epoch 10 and 50. Pseudo-clusters are sorted in increasing entropy values. As can be seen, there is an improvement between epoch 10 and 50. The area under the entropy curves is indeed smaller at epoch 50 (0.24 of mean entropy) than at epoch 10 (0.39 of mean entropy), meaning that entropy values are globally smaller. Following this first assessment, we have tried to understand better how the real classes were distributed within each pseudo-cluster. To do so, we focused on the majority class among each cluster, i.e., the most frequent label (among the real classes) in the set of 3D points belonging to the pseudo-cluster. We have observed that, after 50 epochs of training, for 80% of the pseudo-clusters, the proportion of the majority class was higher than 93 %. These results confirmed the relevance of the proposed user-guided strategy to automatically map a pseudo-cluster onto the majority real class for the evaluation, as stated in the method description (see Section 2.3).

After having studied the training behavior of the DC3DCD method, we will now compare it to the state-of-the-art on the testing set of both simulated and real datasets.

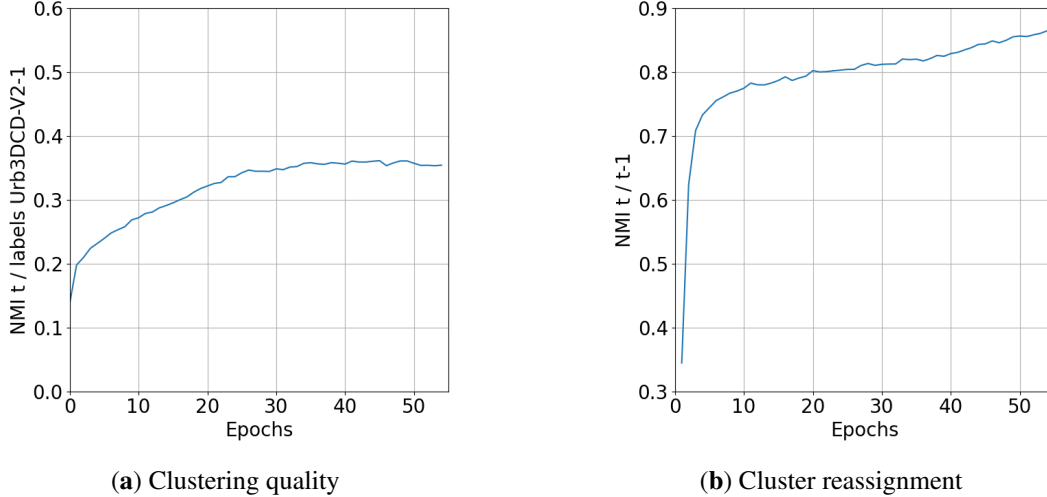


Figure 4: **Analysis of the behavior of DC3DCD during the training.** The evolution of clustering quality (a) is given thanks to the NMI between the clustering and the real labels of Urb3DCD-V2 dataset. The NMI between the clustering at epoch t and the clustering at epoch $t - 1$ gives the cluster reassignment (b).

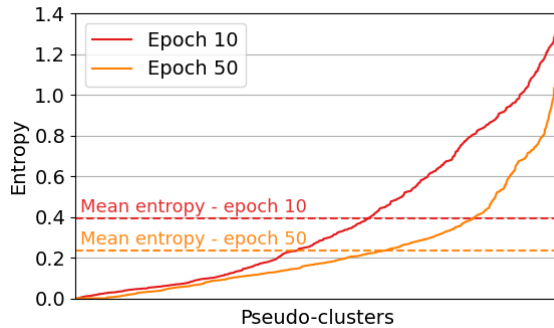


Figure 5: **Pseudo-cluster entropy at epoch 10 and 50.** The entropy is a measure of purity of pseudo-clusters. The lower the entropy, the purer the pseudo-cluster. Pseudo-clusters are sorted in increasing entropy values.

3.3 Results on simulated Urb3DCD dataset

Quantitative evaluation of DC3DCD on the simulated Urb3DCD-V2-1 dataset is given in Table 1 and Table 2. In these tables, we also recall supervised results for the sake of comparison. Let us first analyze DC3DCD results without hand-crafted features (two first lines of the bottom part of Table 1 and Table 2). As can be seen, results for both *Siamese KPConv* and *Encoder Fusion SiamKPConv* back-bones are rather low. Indeed, while requiring the same annotation effort, k -means algorithm trained on the same hand-crafted as the RF method proposed in Tran et al. [2018] provides better results (cf. first line of middle part in Table 1). However, these results are interesting because the two experimented back-bones provide significantly different results. In particular, *Encoder Fusion SiamKPConv* ends up with a $mIoU_{ch}$ 1.5 times higher than *Siamese KPConv*. While in a supervised setting, the improvement of *Encoder Fusion SiamKPConv* was of 5 points of $mIoU_{ch}$, in the unsupervised context the choice of the architecture seems even more crucial.

Then, when hand-crafted features are added to the input of the network, results are largely improved (cf. the two last lines of Table 1). While DC3DCD with *Siamese KPConv* architecture and hand-crafted features provides results comparable to the k -means algorithm, DC3DCD yields compelling results with both hand-crafted features and the *Encoder Fusion SiamKPConv* architecture. Indeed, in this configuration there is more than 15 points of $mIoU_{ch}$ of improvement compared to k -means. Furthermore, DC3DCD with this configuration is better than a fully supervised RF, and provides results comparable with fully supervised deep architectures trained on 2.5D rasterization of 3D PCs.

	Method	mAcc (%)	mIoU _{ch} (%)
Supervised	Siamese KPConv [de Gélis et al., 2023a]	91.21 ± 0.68	80.12 ± 0.02
	Encoder Fusion SiamKPConv [de Gélis et al., 2023b]	94.23 ± 0.88	85.19 ± 0.24
	DSM-Siamese	80.91 ± 5.29	57.41 ± 3.77
	DSM-FC-EF	81.47 ± 0.55	56.98 ± 0.79
	RF [Tran et al., 2018]	65.82 ± 0.05	52.37 ± 0.10
Weakly sup.	<i>k</i> -means	56.15 ± 0.62	41.46 ± 0.53
	<i>Encoder Fusion SiamKPConv</i> (batch size 10)	29.03 ± 22.46	12.84 ± 18.49
	<i>Encoder Fusion SiamKPConv</i> (batch size 2)	53.09 ± 3.73	36.60 ± 3.18
	DC3DCD <i>Siamese KPConv</i>	28.28 ± 3.73	14.43 ± 3.70
	DC3DCD <i>Encoder Fusion SiamKPConv</i>	52.30 ± 2.41	37.75 ± 2.11
	DC3DCD <i>Siamese KPConv</i> (with input features)	54.91 ± 5.45	42.27 ± 6.64
	DC3DCD <i>Encoder Fusion SiamKPConv</i> (with input features)	68.45 ± 1.10	57.06 ± 0.41

Table 1: **Quantitative evaluation of DC3DCD on Urb3DCD-V2 low density LiDAR dataset.** *Top:* supervised methods. DSM-based methods are adaptation of Daudt et al. [2018] networks to DSM inspired by Zhang et al. [2019] and RF refers to Random Forests. *Middle:* Weakly supervised methods with *k*-means and *Encoder Fusion SiamKPConv* results using 7 training cylinders in the training and validation set (equivalent to about 50,000 annotated points). *Bottom:* Weakly supervised methods with our proposed DC3DCD evaluated in 4 different settings: with *Siamese KPConv* or *Encoder Fusion SiamKPConv* architectures and with or without the addition of 10 hand-crafted features as input to the network.

Thereby, providing hand-crafted features is an important step in unsupervised settings. One possible interpretation is that the unsupervised version is very tricky to train in reason of the large number of possible local minima. Adding hand-crafted features probably helps the initialization to be closer to the global minimum.

Notice that the *Encoder Fusion SiamKPConv* in a weakly supervised setting provides rather low results given the higher annotation effort required (about 50,000 annotated points). Results with a batch size of 10 are not stable. This is explained by the fact that only one batch is seen per epoch, and the same learning rate scheduler as with a batch size of 2 is used. Thus, this training is more prone to fall in a local minimum. Even with a reduced batch size, leading to more stable results, we can see the benefit of using DC3DCD for the training of *Encoder Fusion SiamKPConv* network because the effort of annotation is lower.

Two different examples are given for a qualitative assessment of the method in Figures 6 and 7. As visible in Figure 7, main changes (e.g., new buildings or demolitions) seem quite well retrieved by the *k*-means and both DC3DCD configurations. However, when going more into details, some misclassifications can be seen on new building facades (Figure 6) or vegetation. For new building facades, a slight improvement over *k*-means is reached by DC3DCD, but it is still not perfect. The *k*-means technique has the same tendency as the RF method (see de Gélis et al. [2023a]) and confuses small new buildings with new vegetation, surely because they have the same height as visible in Figure 6. As depicted in Table 2, main difficulties of the DC3DCD method concern vegetation growth and missing vegetation. Note that this was already the most difficult classes in the supervised context. The missing vegetation is almost always confused with demolition in DC3DCD with hand-crafted input features and the *Encoder Fusion SiamKPConv* architecture. This is even worse with the *k*-means and missing vegetation is never predicted with DC3DCD without hand-crafted input features. However, this make sense, since the ‘missing vegetation’ and ‘demolition’ classes are both negative changes. Surprisingly, mobile objects are quite well retrieved, especially for DC3DCD with hand-crafted input features and the *Encoder Fusion SiamKPConv* architecture (Table 2).

3.4 Results on real AHN-CD dataset

Urb3DCD being a synthetic dataset, additional experiments are needed to assess the behavior of our method on real data. We consider here the AHN-CD dataset in two settings. First, we conduct a multi-class change segmentation scenario as done previously with Urb3DCD. Then, to allow comparison with other unsupervised deep models for 3D PC change detection, we reduce the multi-class scenario to a bi-class problem, where the results consist only in the presence or absence of a change (and not the type of change).

3.4.1 Multi-class change segmentation

Concerning the real AHN-CD dataset, quantitative results on the manually annotated testing set are given in Table 3, and Table 4 for per class results. While this dataset may contain some registrations errors, we have not observed any significant effect on the change segmentation results. For comparison purpose, we also provide results of supervised methods. However, we recall that they have been trained on the semi-automatically annotated AHN-CD dataset

	Method	Per class IoU (%)						
		Unchanged	New building	Demolition	New veg.	Veg. growth	Missing veg.	Mobile Object
Supervised	SKPConv [de Gélis et al., 2023a]	95.82 ± 0.48	86.68 ± 0.47	78.66 ± 0.47	93.16 ± 0.27	65.17 ± 1.37	65.46 ± 0.93	91.55 ± 0.60
	EFSKPCConv [de Gélis et al., 2023b]	97.47 ± 0.04	96.68 ± 0.30	82.29 ± 0.16	96.52 ± 0.03	67.76 ± 1.51	73.50 ± 0.81	94.37 ± 0.54
	DSM-Siamese	93.21 ± 0.11	86.14 ± 0.65	69.85 ± 1.46	70.69 ± 1.35	8.92 ± 15.46	60.71 ± 0.74	8.14 ± 5.42
	DSM-FC-EF	94.39 ± 0.12	91.23 ± 0.31	71.15 ± 0.99	68.56 ± 3.92	1.89 ± 2.82	62.34 ± 1.23	46.70 ± 3.49
	RF [Tran et al., 2018]	92.72 ± 0.01	73.16 ± 0.02	64.60 ± 0.06	75.17 ± 0.06	19.78 ± 0.30	7.78 ± 0.02	73.71 ± 0.63
Weakly sup.	<i>k</i> -means	91.82 ± 0.05	70.46 ± 0.25	59.83 ± 0.11	59.20 ± 0.48	6.00 ± 0.19	0.00 ± 0.00	53.26 ± 3.19
	EFSKPCConv (b. s. 10)	58.38 ± 46.55	13.22 ± 16.83	26.15 ± 23.54	11.04 ± 19.12	0.41 ± 0.71	7.29 ± 11.99	19.48 ± 33.46
	EFSKPCConv (b. s. 2)	89.88 ± 0.53	29.26 ± 16.83	48.66 ± 2.57	52.91 ± 9.19	7.59 ± 6.40	14.35 ± 15.16	66.84 ± 5.42
	DC3DCD SKPConv	84.51 ± 0.70	13.33 ± 3.05	29.50 ± 13.19	40.31 ± 9.15	3.03 ± 1.80	0.08 ± 0.01	0.33 ± 0.29
	DC3DCD EFSKPCConv	90.90 ± 0.79	64.06 ± 5.13	54.35 ± 3.84	58.14 ± 20.03	1.45 ± 2.05	0.94 ± 0.78	47.57 ± 2.58
	DC3DCD SKPConv (i. f.)	92.90 ± 0.21	76.61 ± 2.09	67.22 ± 2.63	61.33 ± 10.07	8.66 ± 6.54	16.39 ± 14.95	23.44 ± 40.54
	DC3DCD EFSKPCConv (i. f.)	93.96 ± 0.11	79.26 ± 0.68	67.88 ± 0.49	75.34 ± 2.81	19.48 ± 4.00	20.29 ± 2.90	80.10 ± 3.16

Table 2: **Per-class IoU scores of DC3DCD on Urb3DCD-V2 low density LiDAR dataset.** *Top*: supervised methods. DSM-based methods are adaptation of Daudt et al. [2018] networks to DSM inspired by Zhang et al. [2019] and RF refers to Random Forests. *Middle*: Weakly supervised methods with *k*-means and *Encoder Fusion SiamKPConv* results using 7 training cylinders in the training and validation set (equivalent to about 50,000 annotated points). *Bottom*: Weakly supervised methods with our proposed DC3DCD evaluated in 4 different settings: with *Siamese KPConv* (SKPConv) or *Encoder Fusion SiamKPConv* (EFSKPCConv) architectures and with or without the addition of 10 hand-crafted features as input to the network. Veg. stands for vegetation; b. s. for batch size; i. f. for input features.

	Method	mAcc (%)	mIoU _{ch} (%)
Supervised	Siamese KPConv [de Gélis et al., 2023a]	85.65 ± 1.55	72.95 ± 2.05
	Encoder Fusion SiamKPConv [de Gélis et al., 2023b]	90.26 ± 0.22	75.00 ± 0.74
	DSM-Siamese	50.87 ± 1.15	30.96 ± 2.48
	DSM-FC-EF	71.47 ± 1.43	45.57 ± 0.98
	RF [Tran et al., 2018]	47.94 ± 0.02	29.45 ± 0.02
WS	<i>k</i> -means	70.07 ± 0.56	53.12 ± 0.79
	DC3DCD <i>Encoder Fusion SiamKPConv</i> (with input features)	83.18 ± 1.10	66.69 ± 2.19

Table 3: **Qualitative assessment of DC3DCD on the manually annotated sub-part of AHN-CD dataset.** *Top*: supervised methods. DSM-based methods are adaptation of Daudt et al. [2018] networks to DSM inspired by Zhang et al. [2019] and RF refers to Random Forests. In supervised settings, the training is performed on the semi-automatically annotated AHN-CD dataset containing some errors (see de Gélis et al. [2023a]). *Bottom*: Weakly supervised methods with *k*-means and our proposed DC3DCD with *Encoder Fusion SiamKPConv* architecture and with the addition of 10 hand-crafted features as input to the network.

containing several ground truth errors [de Gélis et al., 2023a]. This explains lower results of the RF compared to the *k*-means which have been mapped onto real classes using the manually annotated set (as for DC3DCD method). As already observed with the simulated dataset, we can see that DC3DCD provides better results than the *k*-means algorithm. Figure 8 shows that main changes are well retrieved for both methods. However, in the *k*-means results, larger objects of the clutter class such as trucks are mixed up with buildings. There are also lots of misclassifications in unchanged vegetation and unchanged building facades (see region of interest in Figure 8f). As far as DC3DCD is concerned, unchanged vegetation is well classified. A few mistakes are visible in some ‘new clutter’ objects. We recall that this class is a mix of a lot of objects, from vegetation to cars or garden sheds, surely explaining why its classification score is lower. Complementary results on a larger AHN-CD testing tile (1 km × 1.2 km corresponding to ca. 65 million points) are shown in Figure 9. The ground truth is given by the semi-automatic process detailed in de Gélis et al. [2023a]. The mapping onto the real classes is performed using this ground truth for both *k*-means method and DC3DCD. As visible in this example, most of ‘new clutter’ class objects are omitted or mixed up with the new building class, also the demolition class is totally omitted by the *k*-means algorithm (Figure 9d). In the DC3DCD results in Figure 9e, clutter class seems better retrieved, even though it is not perfect implying the main differences with the ground truth (Figure 9g). In the areas of interest depicted by the black rectangles in Figure 9, we observe that DC3DCD seems to better adapt to the user context (i.e., by the ground truth defined by the user) than the *k*-means, even though the same ground truth-guided mapping step has been performed. Indeed, here buildings are not set as new in the ground truth and in DC3DCD, conversely to *k*-means. Finally, on this tile, if we compare to the ground truth, DC3DCD obtains 55.91% of mIoU_{ch}, while the *k*-means only 24.63%.

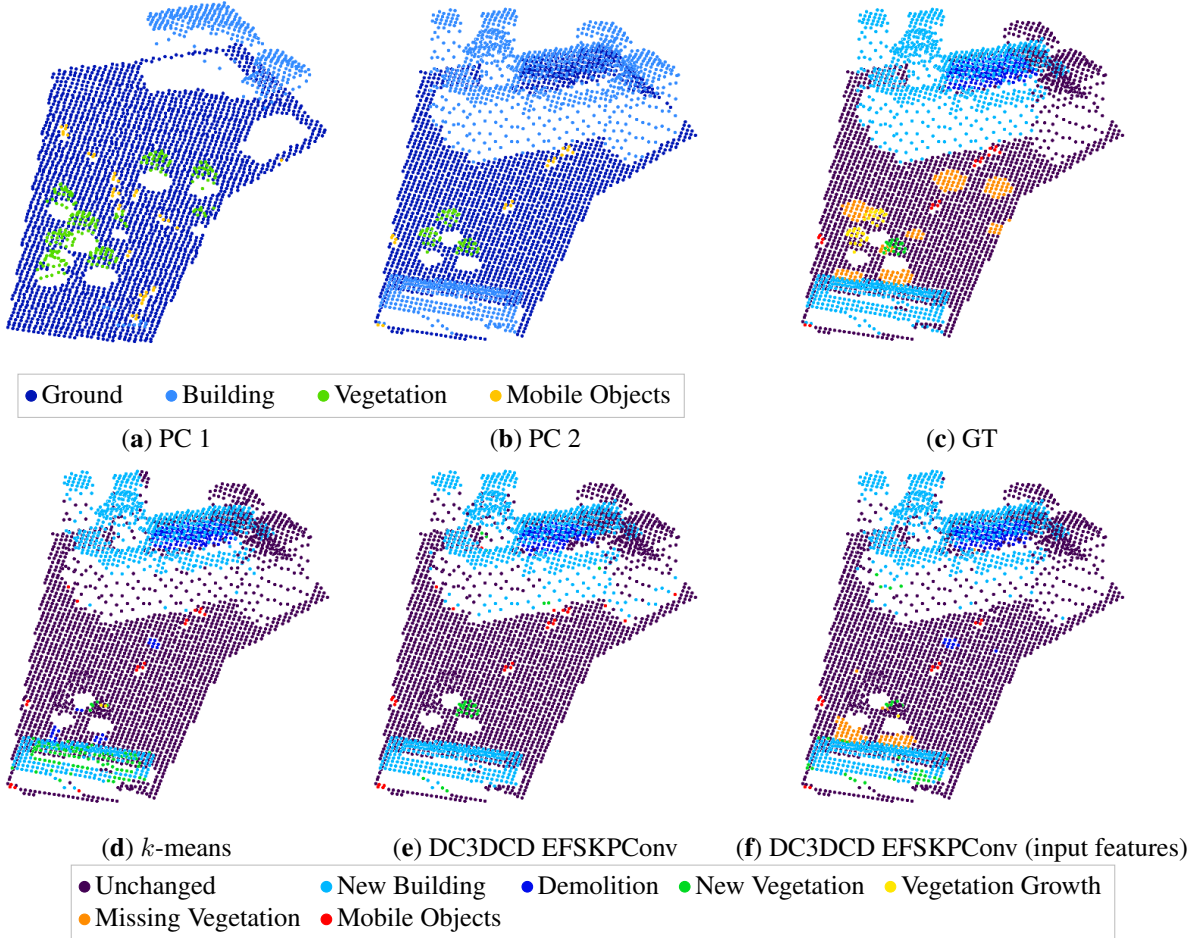


Figure 6: **Visual change detection results on Urb3DCD-V2 low density LiDAR sub-dataset (area 1):** (a-b) the two input point clouds; (c) ground truth (GT): simulated changes; (d) k -means results; (e) DC3DCD with the *Encoder Fusion SiamKPCConv* architecture results; (f) DC3DCD with the *Encoder Fusion SiamKPCConv* architecture and the addition of 10 hand-crafted features as input results.

3.4.2 Binary change detection

To enable comparison with other state-of-the-art methods in unsupervised deep learning, we conduct some experiments in a binary change segmentation (a.k.a. change detection) setup. The results for the manually annotated sub-part of AHN-CD are given in Table 5. For these results, DC3DCD employs user-guided mapping directly for the binary setup (changed and unchanged classes). As evident from these quantitative results, DC3DCD outperforms other fully unsupervised methods significantly. However, it does require 1,000 annotations for mapping the pseudo-clusters to the real classes. Our weakly supervised approach appears as a relevant compromise between supervised methods (here Siamese KPCConv and Encoder Fusion SiamKPCConv) providing high accuracy at the cost of very expensive annotation (millions of points) and unsupervised ones (here SSL-DCVA and SSST-DCVA) that do not need any annotations but achieve much lower accuracy.

4 Discussion

In this paper, we have proposed an unsupervised change detection method with a weakly user-guided mapping to real classes providing convincing results. Unsupervised 3D PCs change detection is still open and complex and in the following, we point out some observations and discussions about possible improvements.

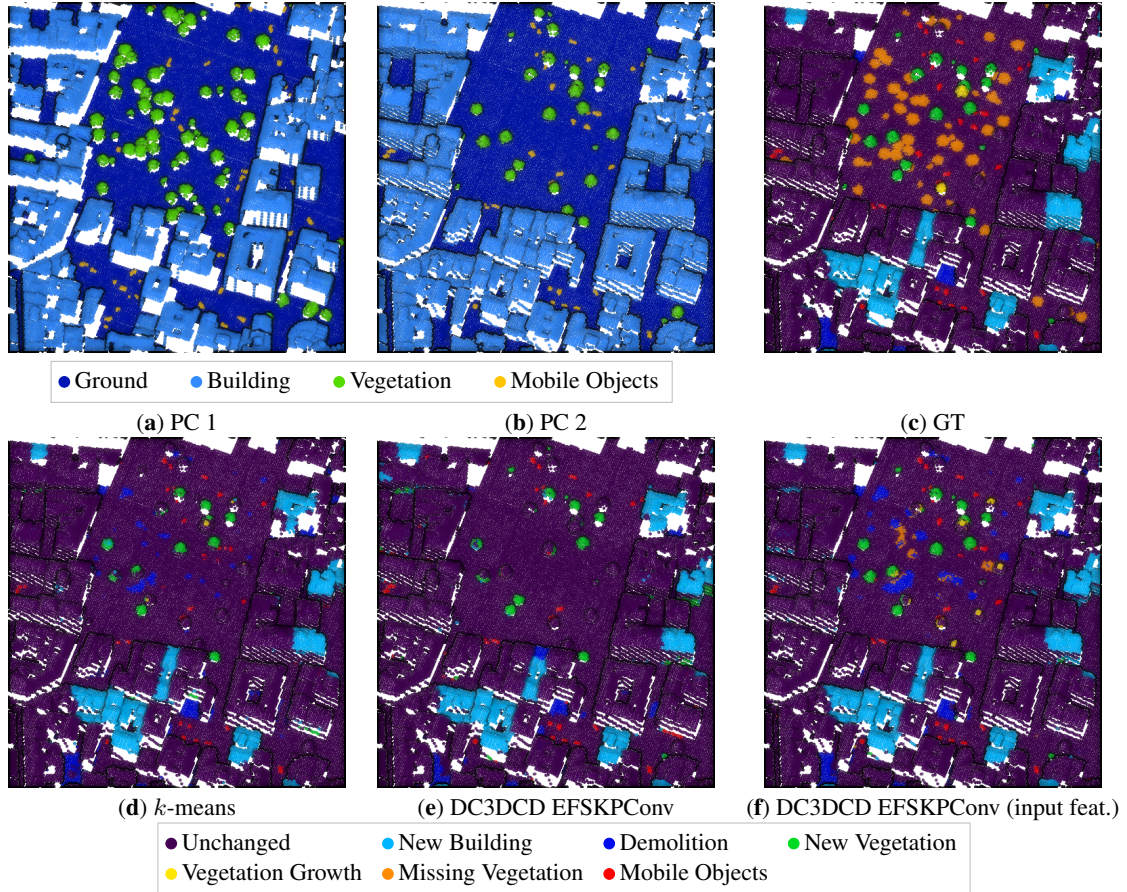


Figure 7: **Visual change detection results on Urb3DCD-V2 low density LiDAR sub-dataset (area 2):** (a-b) the two input point clouds; (c) ground truth (GT): simulated changes; (d) k -means results; (e) DC3DCD with the *Encoder Fusion SiamKPCConv* architecture results; (f) DC3DCD with the *Encoder Fusion SiamKPCConv* architecture and 10 hand-crafted input features.

Method	Per class IoU (%)			
	Unchanged	New building	Demolition	New clutter
Supervised				
Siamese KPCConv [de Gélis et al., 2023a]	89.75 ± 2.18	82.77 ± 5.38	86.44 ± 0.88	46.65 ± 0.16
Encoder Fusion SiamKPCConv [de Gélis et al., 2023b]	94.79 ± 0.34	95.31 ± 1.95	88.87 ± 1.59	41.16 ± 1.30
DSM-Siamese	77.10 ± 1.51	76.77 ± 0.79	4.91 ± 8.33	11.20 ± 1.71
DSM-FC-EF	70.77 ± 1.13	90.32 ± 0.61	30.58 ± 1.76	15.81 ± 0.81
RF [Tran et al., 2018]	78.24 ± 0.00	74.64 ± 0.03	0.00 ± 0.00	13.72 ± 0.06
WS				
k -means	84.13 ± 0.49	83.13 ± 0.89	55.40 ± 0.50	20.84 ± 1.00
DC3DCD <i>Encoder Fusion SiamKPCConv</i> (with input features)	91.34 ± 1.21	89.91 ± 0.72	69.52 ± 4.97	40.63 ± 0.97

Table 4: **Per class IoU DC3DCD results on the manually annotated testing part of AHN-CD dataset given in %.** *Top:* supervised methods. In supervised settings, the training is performed on the semi-automatically annotated AHN-CD dataset containing some errors (see de Gélis et al. [2023a]). *Bottom:* Weakly supervised methods with k -means and our proposed DC3DCD with *Encoder Fusion SiamKPCConv* architecture and with the addition of 10 hand-crafted features as input to the network.

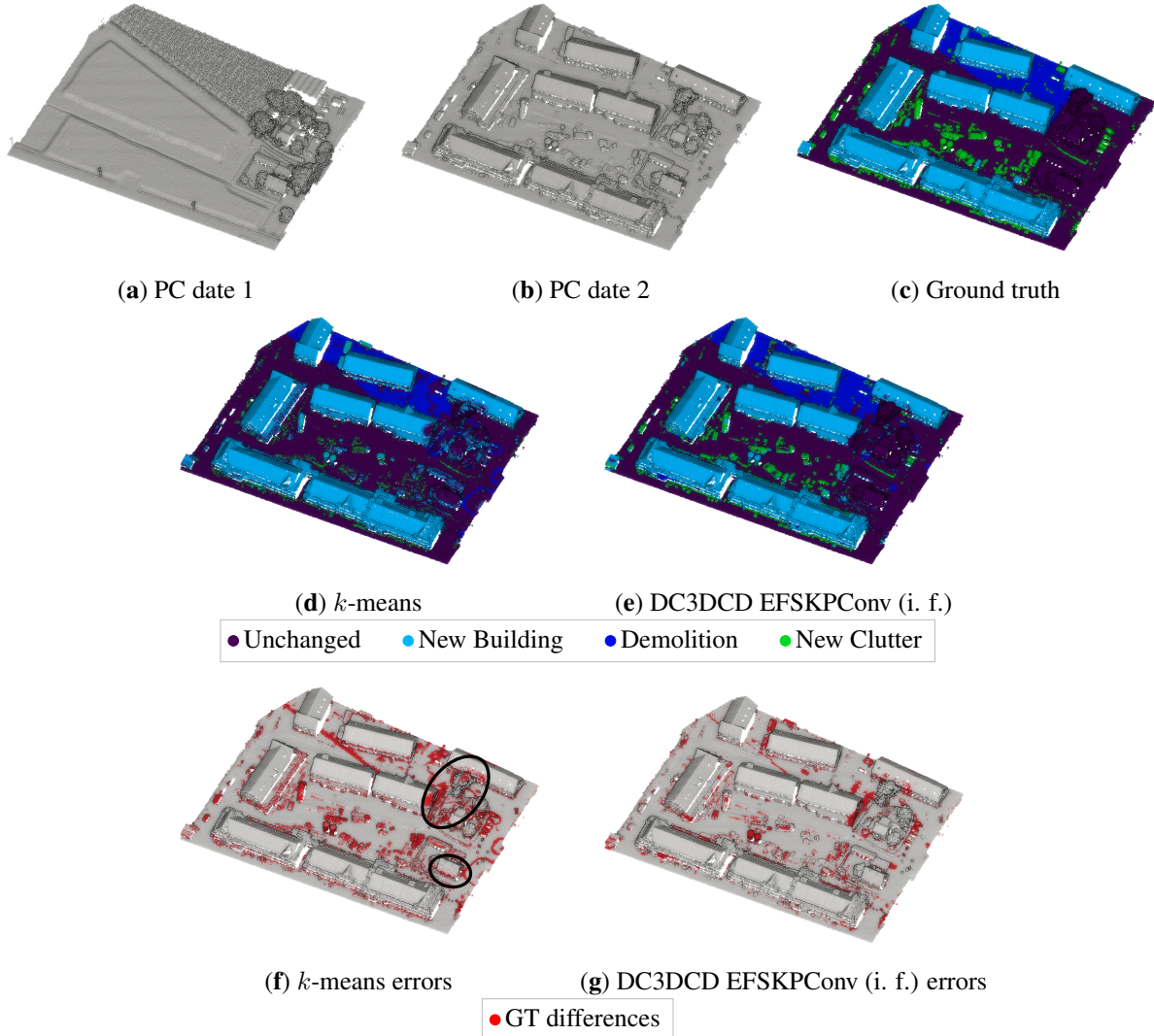


Figure 8: **Qualitative results on the manually annotated sub-part of AHN-CD dataset:** (a-b) PCs at date 1 and 2; (c) ground truth; k -means results (d) and errors (f); DC3DCD results (e) and errors (g) using the *Encoder Fusion SiamKPCConv* architecture and the 10 hand-crafted features in input. Regions of interest specifically discussed in the text are highlighted with ellipses.

4.1 Importance of network’s architectures and input features

We saw in the result section that the choice of the back-bone architecture and the addition of hand-crafted features as input along with 3D point coordinates are crucial. This is in agreement with the original publication of DeepCluster, where image gradients are provided as input to obtain accurate results [Caron et al., 2018]. These results in an unsupervised context also emphasizes conclusions of de Gélis et al. [2023b] on the necessity of applying convolution on features difference. To explain this, let us note that the unsupervised context is a largely unconstrained problem. While the annotation allows counterbalancing architectures weaknesses, this is indeed no longer possible for the unsupervised setting. Thereby the choice of an architecture that more specially extracts change-related features through convolutions of difference of features from both inputs at multiple scales, and the addition of well-designed hand-crafted features, allows guiding the training of the network toward a relevant minimum, leading to an accurate change segmentation.

	Method	mAcc (%)	IoU (%)	
			Unchanged	Changed
Sup.	Siamese KPConv [de Gélis et al., 2023a]	97.08	95.39	92.95
	Encoder Fusion SiamKPConv [de Gélis et al., 2023b]	96.75	94.79	92.10
Unsup.	SSL-DCVA [de Gélis et al., 2023c]	85.20	78.91	69.38
	SSST-DCVA [de Gélis et al., 2023c]	81.88	70.02	63.85
W. Sup	DC3DCD <i>Encoder Fusion SiamKPConv</i> (with input features)	94.43	91.24	86.96

Table 5: **Quantitative comparison on a binary change segmentation task on the manually annotated sub-part of AHN-CD dataset.**

4.2 Improving DC3DCD with contrastive learning

As mentioned, the problem in an unsupervised setting is to train a network to extract appropriate features for a specific task. In a task involving comparison of similar and dissimilar data (like change detection task), the contrastive loss is often used to force the network to extract identical features for similar data. Therefore, we explore here how to force the network to predict similar features for unchanged areas. To do so, we propose to introduce the following contrastive term in the loss function:

$$\mathcal{L}_{cont} = 0.5 \times y_{sim} \times F_{CD}^2 \quad \text{with} \quad y_{sim} = \begin{cases} 1 & \text{if similar} \\ 0 & \text{else.} \end{cases} \quad (5)$$

where F_{CD} is the L_2 -norm of output features and y_{sim} is the similarity term (set to 1 for unchanged points, and 0 elsewhere). Using this contrastive term in the loss aims at forcing to 0 change-related features in unchanged areas. To test this idea, we combine the contrastive loss in Equation 5 with the deep clustering loss (NLL using the pseudo-label) taking the mean, and train the *Encoder Fusion SiamKPConv* network since it gave the best results.

We first carried out experiments by taking the similarity y_{sim} from the ground truth (as y_{sim} is not available in practice, we first test the idea by taking real values of y_{sim}). Results were really convincing since, as visible in Table 6 and Table 7, DC3DCD reached 73.51% of $mIoU_{ch}$ without the use of hand-crafted features and 82.63% of $mIoU_{ch}$ with the use of hand-crafted features on Urb3DCD-V2-1 dataset. We recall that on this dataset and in a fully supervised setting, *Siamese KPConv* and *Encoder Fusion SiamKPConv* networks obtained 80.12% and 85.19% of $mIoU_{ch}$ respectively. Thus, the addition of the contrastive part allows meeting fully supervised results (in an ideal case where y_{sim} is known).

This first experience validated the idea of using the contrastive loss. However in practice, y_{sim} needs to be estimated. To obtain the similarity y_{sim} , we first used the significant changes given by Multi-Scale Model-to-Model Cloud Comparison (M3C2) [Lague et al., 2013] or a binary thresholding of cloud-to-cloud (C2C) distance [Girardeau-Montaut et al., 2005]. Results are mitigated (see Table 6 and Table 7) since, without hand-crafted input features, the best results obtained using M3C2 for y_{sim} allow us to improve by only 2% the mean of IoU over classes of change obtained with DC3DCD. With hand-crafted input features, results are worsened when the contrastive term is added during the training (using y_{sim} based on M3C2, obtained $mIoU_{ch}$ is 46.42%).

Another idea is to rely on multi-task learning [Vandenhende et al., 2021, Zhang and Yang, 2021]: a multi-task framework based on DC3DCD that jointly extracts mono-date features that can be used for similarity computation has been designed. As illustrated in Figure 10, we added decoders for mono-date semantic segmentation to the back-bone architectures to also obtain semantic segmentation of PCs. Both *Siamese KPConv* and *Encoder Fusion SiamKPConv* have encoders to extract mono-date features, therefore we just added a decoder taking as input these mono-date features instead of feature differences for *Siamese KPConv* for example. Thereby, we used the same idea as before to train the network but with two separate clusterings, performed on output features of the change decoder on one side, as in previous experiments, and on output features of mono-date decoders on the other side. This results in both change pseudo-labels and mono-date pseudo-labels which are used to modulate change encoder-decoder and mono-date encoders-decoders respectively. In practice, we shared trainable parameters between mono-date encoders and decoders. We trained first the semantic segmentation part and then apply a binary clustering (using k -means) on the nearest point mono-date features difference to obtain the similarity y_{sim} used in the contrastive term of the change detection loss. Concerning, the number of pseudo-clusters for mono-date $K_{mono-date}$, 4 and 500 have been tested (4 is the number of semantic segmentation classes in Urb3DCD-V2 dataset, 500 is considered as a sample large bound). While semantic segmentation scores, using the same user-guided mapping for mono-date semantic segmentation, are very promising (90.79% of mean of IoU ($mIoU$) on the 4 semantic segmentation classes of Urb3DCD-V2 with hand-crafted input features and $K_{mono-date} = 500$), using the associated y_{sim} still leads to unsatisfactory results (see Table 6 and Table 7). Indeed, when $K_{mono-date}$ is set to 500, we obtain 50.14% of $mIoU_{ch}$ (with hand-crafted features) which

	Method	i. f.	y_{sim}	mAcc (%)	mIoU _{ch} (%)
Sup.	SKPConv [de Gélis et al., 2023a]			91.21 ± 0.68	80.12 ± 0.02
	EFSKPCConv [de Gélis et al., 2023b]			94.23 ± 0.88	85.19 ± 0.24
Weakly supervised	DC3DCD EFSKPCConv			52.30 ± 2.41	37.75 ± 2.11
	DC3DCD-V2 EFSKPCConv		GT	83.45 ± 2.22	73.51 ± 3.74
	DC3DCD-V2 EFSKPCConv		M3C2 [Lague et al., 2013]	54.01 ± 3.54	39.59 ± 4.18
	DC3DCD-V2 EFSKPCConv		C2C [Girardeau-Montaut et al., 2005]	39.74 ± 1.84	25.57 ± 1.97
	DC3DCD-V2 EFSKPCConv		Multi-task ($K_{seg.sem.} = 4$)	34.31 ± 5.85	19.21 ± 5.81
	DC3DCD-V2 EFSKPCConv		Multi-task ($K_{seg.sem.} = 500$)	47.62 ± 6.76	32.07 ± 6.15
	DC3DCD EFSKPCConv	✓		68.45 ± 1.10	57.06 ± 0.41
	DC3DCD-V2 EFSKPCConv	✓		89.04 ± 0.70	82.63 ± 0.73
	DC3DCD-V2 EFSKPCConv	✓		58.80 ± 2.14	46.42 ± 2.45
	DC3DCD-V2 EFSKPCConv	✓		42.01 ± 0.67	28.04 ± 0.60
DC3DCD-V2 EFSKPCConv	✓		53.04 ± 8.22	38.90 ± 8.51	
DC3DCD-V2 EFSKPCConv	✓		62.95 ± 1.81	50.14 ± 3.85	

Table 6: **Quantitative evaluation of DC3DCD-V2 on Urb3DCD-V2 low density LiDAR dataset.** *Top:* supervised methods. *Middle:* Weakly supervised methods with our proposed DC3DCD and DC3DCD-V2 with Encoder Fusion SiamKPCConv architecture without the addition of 10 hand-crafted features as input to the network. *Bottom:* Weakly supervised methods with our proposed DC3DCD and DC3DCD-V2 with Encoder Fusion SiamKPCConv architecture and with the addition of 10 hand-crafted features (i. f.) as input to the network.

	Method	i. f.	y_{sim}	Per class IoU (%)						
				Unchanged	New building	Demolition	New veg.	Veg. growth	Missing veg.	Mobile Object
Sup.	SKPConv			95.82 ± 0.48	86.68 ± 0.47	78.66 ± 0.47	93.16 ± 0.27	65.17 ± 1.37	65.46 ± 0.93	91.55 ± 0.60
	EFSKPCConv			97.47 ± 0.04	96.68 ± 0.30	82.29 ± 0.16	96.52 ± 0.03	67.76 ± 1.51	73.50 ± 0.81	94.37 ± 0.54
Weakly supervised	DC3DCD			90.90 ± 0.79	64.06 ± 5.13	54.35 ± 3.84	58.14 ± 20.03	1.45 ± 2.05	0.94 ± 0.78	47.57 ± 2.58
	DC3DCD-V2		GT	97.28 ± 0.10	93.66 ± 1.30	75.24 ± 4.34	83.78 ± 6.00	49.52 ± 7.00	53.60 ± 11.98	85.28 ± 3.54
	DC3DCD-V2		M3C2	93.02 ± 0.03	75.05 ± 5.28	57.43 ± 2.03	69.02 ± 5.77	10.45 ± 8.60	4.47 ± 4.22	21.11 ± 10.22
	DC3DCD-V2		C2C	90.73 ± 0.45	64.93 ± 3.79	56.52 ± 3.74	10.76 ± 5.80	0.41 ± 0.56	0.44 ± 0.51	20.37 ± 6.96
	DC3DCD-V2		Multi-task ($K_{seg.sem.} = 4$)	87.15 ± 2.38	29.55 ± 16.82	39.72 ± 7.84	28.11 ± 2.95	0.00 ± 0.00	0.08 ± 0.09	17.78 ± 11.09
	DC3DCD-V2		Multi-task ($K_{seg.sem.} = 500$)	88.56 ± 2.11	40.44 ± 12.79	45.16 ± 12.73	50.12 ± 6.53	4.03 ± 5.09	0.43 ± 1.19	51.93 ± 6.90
	DC3DCD	✓		93.96 ± 0.11	79.26 ± 0.68	67.88 ± 0.49	75.34 ± 2.81	19.48 ± 4.00	20.29 ± 2.90	80.10 ± 3.16
	DC3DCD-V2	✓		97.73 ± 0.05	94.50 ± 0.20	81.10 ± 0.38	92.22 ± 0.92	61.32 ± 2.39	73.39 ± 1.18	90.12 ± 1.30
	DC3DCD-V2	✓		93.17 ± 0.13	77.48 ± 1.85	65.34 ± 0.55	76.96 ± 5.26	25.65 ± 4.94	0.31 ± 0.54	32.76 ± 4.15
	DC3DCD-V2	✓		92.25 ± 0.15	70.01 ± 2.77	66.56 ± 1.12	27.11 ± 5.78	0.00 ± 0.00	4.59 ± 0.64	0.00 ± 0.00
DC3DCD-V2	✓		91.96 ± 1.10	69.01 ± 7.24	63.07 ± 1.49	42.76 ± 13.31	4.11 ± 6.71	17.23 ± 7.28	31.20 ± 25.63	
DC3DCD-V2	✓		93.68 ± 0.48	78.23 ± 2.94	66.02 ± 1.46	71.49 ± 2.49	0.00 ± 0.00	16.07 ± 4.77	69.06 ± 16.59	

Table 7: **Per class quantitative evaluation of DC3DCD-V2 on Urb3DCD-V2 low density LiDAR dataset.** *Top:* supervised methods. *Middle:* Weakly supervised methods with our proposed DC3DCD and DC3DCD-V2 with Encoder Fusion SiamKPCConv architecture without the addition of 10 hand-crafted features as input to the network. *Bottom:* Weakly supervised methods with our proposed DC3DCD and DC3DCD-V2 with Encoder Fusion SiamKPCConv architecture and with the addition of 10 hand-crafted features (i. f.) as input to the network.

is better than with distance-based methods (M3C2 [Lague et al., 2013] or C2C [Girardeau-Montaut et al., 2005]) but worse than without the contrastive part of the loss. Thereby, computing similarity from the nearest point mono-date features difference does not seem adapted. Two main reasons for this non-success can be advanced: i) the nearest point comparison is not optimal in occluded parts as well as in dense urban areas (which is the case for Urb3DCD datasets that are acquired on models of Lyon city center), and ii) there might be some side effects of the oversegmentation strategy. To explain, the method predicts 500 different mono-date semantic classes (far more than existing real classes). The oversegmentation occurring on the mono-date semantic segmentations leads to splitting each real semantic class into numerous semantic pseudo-classes. In other words, two points that belong to the same real semantic class will very likely be assigned to different semantic pseudo-classes (both pseudo-classes corresponding to the same real class). Since the change information is obtained by comparing the pseudo-classes and not the real ones, the similarity term y_{sim} might be incorrect if the two pseudo-classes are far from each other in the feature space, and thus their difference is classified as changed during the binary clustering step. To counterbalance this oversegmentation issue, we tested using only 4 mono-date pseudo-clusters, but results are even worse, probably due to the fact that the DeepCluster strategy used to train a network requires a number of pseudo-clusters far greater than the number of real classes. Thereby, we are facing here a conflicting situation, where the oversegmentation is needed to obtain an accurate mono-date semantic segmentation, but at the cost of errors in the identification of binary changes by comparing the mono-date semantic segmentations.

Qualitative assessment of these results is supported by Figure 11 and Figure 12. When the similarity comes from the binary change ground truth, visual results really look like the multi-change ground truth (Figure 11f and Figure 12c). Qualitative results of multi-task learning are quite encouraging. Surprisingly, borders of ‘missing vegetation’ seems well retrieved, but the center is still confused with demolition.

All these experiments aim at evaluating the potential of contrastive losses to improve our unsupervised results. Results with the similarity y_{sim} issued from ground truth are very promising since they reach comparable results than the fully supervised networks. However, the method is highly dependent on the quality of this binary change annotation, and in case of mitigated binary annotation, it worsens DC3DCD results. These first perspective experimentation are, to our opinion, encouraging to limit the annotation effort while preserving accurate results. Yet, the estimation of a precise y_{sim} is still an open problem.

5 Conclusion

In this paper, we proposed an unsupervised learning method based on the DeepCluster principle to tackle multiclass change segmentation in raw 3D PCs. Following the unsupervised training, we propose a user-guided mapping of pseudo-clusters to real class in order to better fit to the use case. Given the experiments on both synthetic and real dataset, we saw the importance of the choice of an appropriate architecture to extract valuable change-related features. Also, guiding the network using hand-crafted input features along with 3D points coordinates is advocated.

Using these recommended configuration, our proposed method, DeepCluster 3D Change Detection (DC3DCD), allows obtaining better results than a fully supervised traditional machine learning algorithm relying on hand-crafted features and to reach scores of fully supervised deep networks trained on 2.5D rasterization of PCs. We further proposed to improve DC3DCD by introducing a contrastive loss leading to results comparable to those provided by fully supervised deep networks (89.04% of mean of accuracy).

This last setting is very promising but was considered here in an ideal scenario where the similarity boolean used in the contrastive loss is faultless. The main challenge that remains to be solved is thus to be able to estimate the similarity term directly from the data. Another future work that would be of interest is to consider a multi-level classification scenario, using a hierarchical clustering technique instead of a flat one. Finally, semi-automatic strategies to speed-up labeling the K clusters would also be of high benefit to ease deployment of our method.

Acknowledgements

This research was funded by Magellium, Toulouse and the CNES, Toulouse. This work was granted access to the HPC resources of IDRIS under the allocation 2022-AD011011754R2 made by GENCI.

References

Begüm Demir, Francesca Bovolo, and Lorenzo Bruzzone. Updating land-cover maps by classification of image time series: A novel change-detection-driven transfer learning approach. *IEEE Transactions on Geoscience and Remote Sensing*, 51(1):300–312, 2012.

- Laigen Dong and Jie Shan. A comprehensive review of earthquake-induced building damage detection with remote sensing techniques. *ISPRS Journal of Photogrammetry and Remote Sensing*, 84:85–99, 2013.
- R. Qin, J. Tian, and P. Reinartz. 3D change detection – approaches and applications. *ISPRS Journal of Photogrammetry and Remote Sensing*, 122:41–56, 2016.
- Corné Van Der Sande, Sylvie Soudarissanane, and Kourosh Khoshelham. Assessment of relative accuracy of ahn-2 laser scanning data using planar features. *Sensors*, 10(9):8198–8214, 2010.
- M Bernard, D Decluseau, L Gabet, and P Nonin. 3d capabilities of pleiades satellite. *Int. Arch. Photogramm. Remote Sens. Spatial Inf. Sci.*, 39:B3, 2012.
- Soubirane Jérôme. Shaping the future of earth observation with pléiades neo. In *2019 9th International Conference on Recent Advances in Space Technologies (RAST)*, pages 399–401. IEEE, 2019.
- L Lebègue, E Cazala-Hourcade, F Languille, S Artigues, and O Melet. Co3d, a worldwide one-meter accuracy dem for 2025. *International Archives of the Photogrammetry, Remote Sensing & Spatial Information Sciences*, 2020.
- Uwe Stilla and Yusheng Xu. Change detection of urban objects using 3d point clouds: A review. *ISPRS Journal of Photogrammetry and Remote Sensing*, 197:228–255, 2023.
- U. Okyay, J. Telling, C.L. Glennie, and W.E. Dietrich. Airborne lidar change detection: An overview of earth sciences applications. *Earth-Science Reviews*, 198:102929, 2019.
- Z. Zhang, G. Vosselman, M. Gerke, D. Tuia, and M. Y. Yang. Change detection between multimodal remote sensing data using siamese cnn. *arXiv preprint arXiv:1807.09562*, 2018a.
- Z. Zhang, G. Vosselman, M. Gerke, C. Persello, D. Tuia, and M.Y. Yang. Detecting building changes between airborne laser scanning and photogrammetric data. *Remote sensing*, 11(20):2417, 2019.
- Balázs Nagy, Lóránt Kovács, and Csaba Benedek. Changelogan: A deep network for change detection in coarsely registered point clouds. *IEEE Robotics and Automation Letters*, 6(4):8277–8284, 2021.
- Tao Ku, Sam Galanakis, Bas Boom, Remco C. Veltkamp, Darshan Bangera, Shankar Gangisetty, Nikolaos Stagakis, Gerasimos Arvanitis, and Konstantinos Moustakas. Shrec 2021: 3d point cloud change detection for street scenes. *Computers & Graphics*, 99:192–200, 2021. ISSN 0097-8493. doi:<https://doi.org/10.1016/j.cag.2021.07.004>. URL <https://www.sciencedirect.com/science/article/pii/S0097849321001369>.
- Yue Wang, Yongbin Sun, Ziwei Liu, Sanjay E Sarma, Michael M Bronstein, and Justin M Solomon. Dynamic graph cnn for learning on point clouds. *ACM Transactions On Graphics (TOG)*, 38(5):1–12, 2019.
- Iris de Gélis, Sébastien Lefèvre, and Thomas Corpetti. Siamese kpconv: 3d multiple change detection from raw point clouds using deep learning. *ISPRS Journal of Photogrammetry and Remote Sensing*, 197:274–291, 2023a. ISSN 0924-2716. doi:<https://doi.org/10.1016/j.isprsjprs.2023.02.001>. URL <https://www.sciencedirect.com/science/article/pii/S0924271623000394>.
- Hugues Thomas, Charles R Qi, Jean-Emmanuel Deschaud, Beatriz Marcotegui, François Goulette, and Leonidas J Guibas. Kpconv: Flexible and deformable convolution for point clouds. In *Proceedings of the IEEE/CVF International Conference on Computer Vision*, pages 6411–6420, 2019.
- Iris de Gélis, Thomas Corpetti, and Sébastien Lefèvre. Change detection needs change information: improving deep 3d point cloud change detection. *arXiv preprint arXiv:2304.12639*, 2023b. doi:10.48550/arXiv.2304.12639.
- Abderrazzaq Kharroubi, Florent Poux, Zouhair Ballouch, Rafika Hajji, and Roland Billen. Three dimensional change detection using point clouds: A review. *Geomatics*, 2(4):457–485, 2022.
- Wen Xiao, Hui Cao, Miao Tang, Zhenchao Zhang, and Nengcheng Chen. 3d urban object change detection from aerial and terrestrial point clouds: A review. *International Journal of Applied Earth Observation and Geoinformation*, 118:103258, 2023.
- Sudipan Saha, Francesca Bovolo, and Lorenzo Bruzzone. Unsupervised deep change vector analysis for multiple-change detection in vhr images. *IEEE Transactions on Geoscience and Remote Sensing*, 57(6):3677–3693, 2019.
- Iris de Gélis, Sudipan Saha, Muhammad Shahzad, Thomas Corpetti, Sébastien Lefèvre, and Xiao Xiang Zhu. Deep unsupervised learning for 3d als point clouds change detection. *ISPRS Open Journal of Photogrammetry and Remote Sensing*, 9:100044, 2023c. ISSN 2667-3932. doi:<https://doi.org/10.1016/j.ophoto.2023.100044>. URL <https://www.sciencedirect.com/science/article/pii/S2667393223000157>.
- Mathilde Caron, Piotr Bojanowski, Armand Joulin, and Matthijs Douze. Deep clustering for unsupervised learning of visual features. In *Proceedings of the European Conference on Computer Vision (ECCV)*, pages 132–149, 2018.
- Yazhou Ren, Jingyu Pu, Zhimeng Yang, Jie Xu, Guofeng Li, Xiaorong Pu, Philip S Yu, and Lifang He. Deep clustering: A comprehensive survey. *arXiv preprint arXiv:2210.04142*, 2022.

- Sheng Zhou, Hongjia Xu, Zhuonan Zheng, Jiawei Chen, Jiajun Bu, Jia Wu, Xin Wang, Wenwu Zhu, Martin Ester, et al. A comprehensive survey on deep clustering: Taxonomy, challenges, and future directions. *arXiv preprint arXiv:2206.07579*, 2022.
- Jang Hyun Cho, Utkarsh Mall, Kavita Bala, and Bharath Hariharan. Picie: Unsupervised semantic segmentation using invariance and equivariance in clustering. In *Proceedings of the IEEE/CVF Conference on Computer Vision and Pattern Recognition*, pages 16794–16804, 2021.
- Puzhao Zhang, Maoguo Gong, Hui Zhang, Jia Liu, and Yifang Ban. Unsupervised difference representation learning for detecting multiple types of changes in multitemporal remote sensing images. *IEEE Transactions on Geoscience and Remote Sensing*, 57(4):2277–2289, 2018b.
- Huihui Dong, Wenping Ma, Licheng Jiao, Fang Liu, and LingLing Li. A multiscale self-attention deep clustering for change detection in sar images. *IEEE Transactions on Geoscience and Remote Sensing*, 60:1–16, 2021.
- Sudipan Saha, Patrick Ebel, and Xiao Xiang Zhu. Self-supervised multisensor change detection. *IEEE Transactions on Geoscience and Remote Sensing*, 60:1–10, 2021.
- Jinming Zhang, Xiangyun Hu, and Hengming Dai. Unsupervised learning of als point clouds for 3-d terrain scene clustering. *IEEE Geoscience and Remote Sensing Letters*, 19:1–5, 2021.
- Paul J Besl and Neil D McKay. Method for registration of 3-d shapes. In *Sensor fusion IV: control paradigms and data structures*, volume 1611, pages 586–606. Spie, 1992.
- J MacQueen. Classification and analysis of multivariate observations. In *5th Berkeley Symp. Math. Statist. Probability*, pages 281–297. University of California Los Angeles LA USA, 1967.
- Frank Lin and William W Cohen. Power iteration clustering. In *Proceedings of the 27th International Conference on Machine Learning*, pages 655–662, 2010.
- Mehdi Noroozi and Paolo Favaro. Unsupervised learning of visual representations by solving jigsaw puzzles. In *Computer Vision—ECCV 2016: 14th European Conference, Amsterdam, The Netherlands, October 11–14, 2016, Proceedings, Part VI*, pages 69–84. Springer, 2016.
- Alex Krizhevsky, Ilya Sutskever, and Geoffrey E Hinton. Imagenet classification with deep convolutional neural networks. *Communications of the ACM*, 60(6):84–90, 2017.
- Karen Simonyan and Andrew Zisserman. Very deep convolutional networks for large-scale image recognition. *arXiv preprint arXiv:1409.1556*, 2014.
- Jia Deng, Wei Dong, Richard Socher, Li-Jia Li, Kai Li, and Li Fei-Fei. Imagenet: A large-scale hierarchical image database. In *2009 IEEE Conference on Computer Vision and Pattern Recognition*, pages 248–255, 2009. doi:10.1109/CVPR.2009.5206848.
- Bart Thomee, David A Shamma, Gerald Friedland, Benjamin Elizalde, Karl Ni, Douglas Poland, Damian Borth, and Li-Jia Li. Yfcc100m: The new data in multimedia research. *Communications of the ACM*, 59(2):64–73, 2016.
- Mathilde Caron, Ishan Misra, Julien Mairal, Priya Goyal, Piotr Bojanowski, and Armand Joulin. Unsupervised learning of visual features by contrasting cluster assignments. *Advances in neural information processing systems*, 33: 9912–9924, 2020.
- Iris de Gélis, Zoé Bessin, Pauline Letortu, Marion Jaud, Christophe Delacourt, Stéphane Costa, Olivier Maquaire, Robert Davidson, Thomas Corpetti, and Sébastien Lefèvre. Cliff change detection using siamese kpconv deep network on 3d point clouds. *ISPRS Annals of the Photogrammetry, Remote Sensing and Spatial Information Sciences*, V-3-2022:649–656, 2022. doi:10.5194/isprs-annals-V-3-2022-649-2022. URL <https://www.isprs-ann-photogramm-remote-sens-spatial-inf-sci.net/V-3-2022/649/2022/>.
- Mathilde Caron. *Self-supervised learning of deep visual representations*. PhD thesis, Université Grenoble Alpes, 2021.
- Ahmad Mustapha, Wael Khreich, and Wasim Masr. A deep dive into deep cluster. *arXiv preprint arXiv:2207.11839*, 2022.
- T.H.G. Tran, C. Ressel, and N. Pfeifer. Integrated change detection and classification in urban areas based on airborne laser scanning point clouds. *Sensors*, 18(2):448, 2018.
- David Sculley. Web-scale k-means clustering. In *Proceedings of the 19th international conference on World wide web*, pages 1177–1178, 2010.
- Iris de Gélis, Sébastien Lefèvre, and Thomas Corpetti. Change detection in urban point clouds: An experimental comparison with simulated 3d datasets. *Remote Sensing*, 13(13), 2021. ISSN 2072-4292. doi:10.3390/rs13132629. URL <https://www.mdpi.com/2072-4292/13/13/2629>.

- Rodrigo Caye Daudt, Bertrand Le Saux, and Alexandre Boulch. Fully convolutional siamese networks for change detection. In *2018 25th IEEE International Conference on Image Processing (ICIP)*, pages 4063–4067. IEEE, 2018.
- Michael Kölle, Dominik Laupheimer, Stefan Schmohl, Norbert Haala, Franz Rottensteiner, Jan Dirk Wegner, and Hugo Ledoux. The hessigheim 3d (h3d) benchmark on semantic segmentation of high-resolution 3d point clouds and textured meshes from uav lidar and multi-view-stereo. *ISPRS Journal of Photogrammetry and Remote Sensing*, 1: 100001, 2021.
- D. Lague, N. Brodu, and J. Leroux. Accurate 3D comparison of complex topography with terrestrial laser scanner: Application to the rangitikei canyon (NZ). *ISPRS Journal of Photogrammetry and Remote Sensing*, 82:10–26, 2013.
- Daniel Girardeau-Montaut, Michel Roux, Raphaël Marc, and Guillaume Thibault. Change detection on points cloud data acquired with a ground laser scanner. *International Archives of Photogrammetry, Remote Sensing and Spatial Information Sciences*, 36(part 3):W19, 2005.
- Simon Vandenhende, Stamatios Georgoulis, Wouter Van Gansbeke, Marc Proesmans, Dengxin Dai, and Luc Van Gool. Multi-task learning for dense prediction tasks: A survey. *IEEE transactions on pattern analysis and machine intelligence*, 44(7):3614–3633, 2021.
- Yu Zhang and Qiang Yang. A survey on multi-task learning. *IEEE Transactions on Knowledge and Data Engineering*, 34(12):5586–5609, 2021.

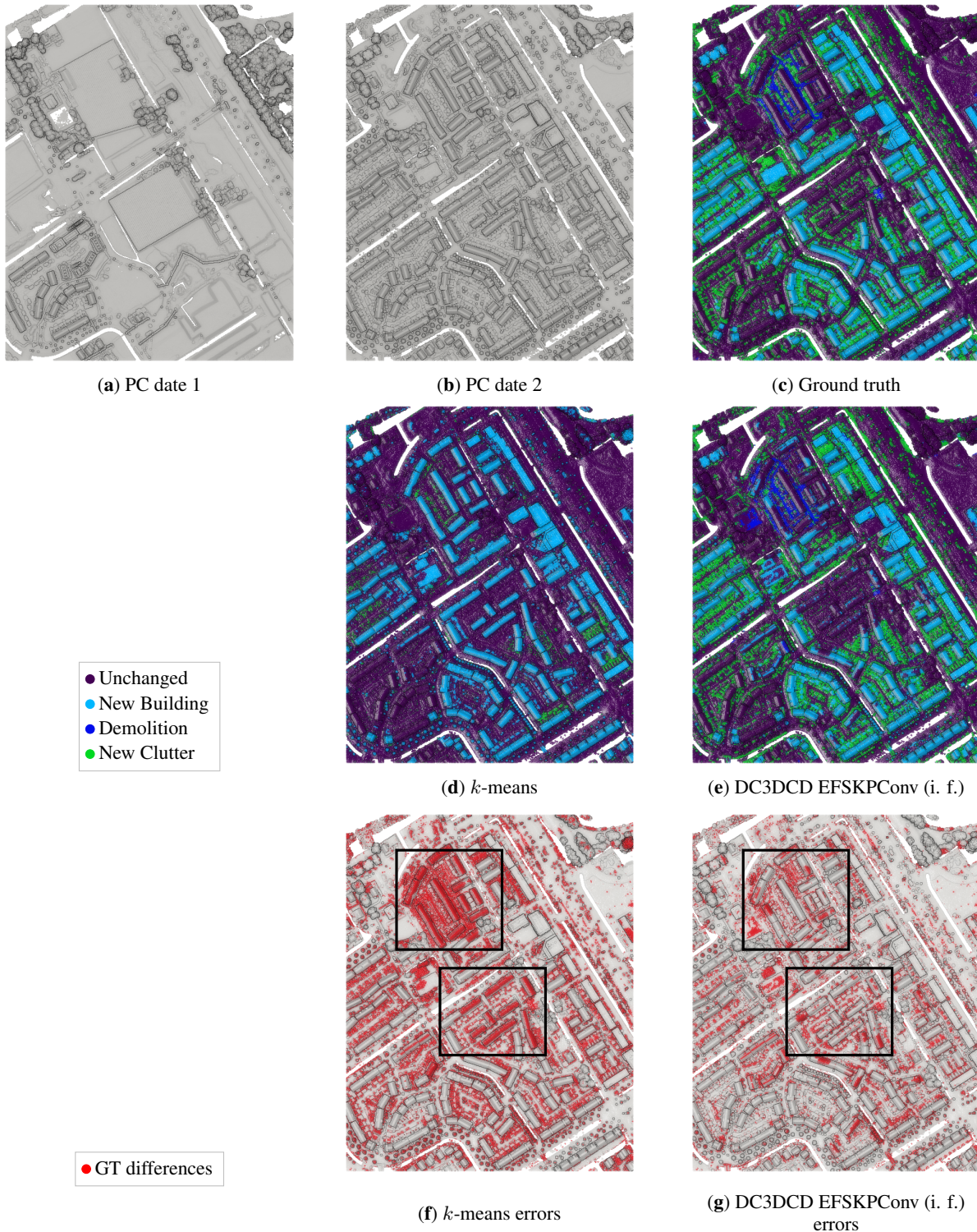


Figure 9: **Qualitative results on the semi-automatically annotated AHN-CD dataset:** (a-b) PCs at date 1 and 2; (c) ground truth; k -means results (d) and corresponding errors (f); DC3DCD results (e) and corresponding errors (g) using the *Encoder Fusion SiamKPCConv* architecture and the 10 hand-crafted features in input. Regions of interest specifically discussed in the text are highlighted with rectangles.

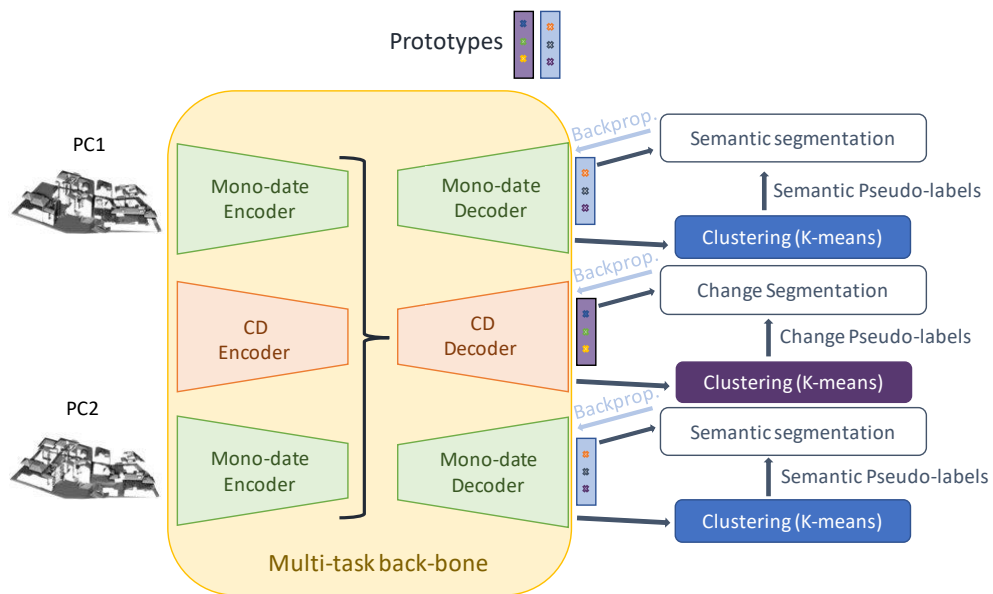


Figure 10: DC3DCD-V2 using multi-task learning.

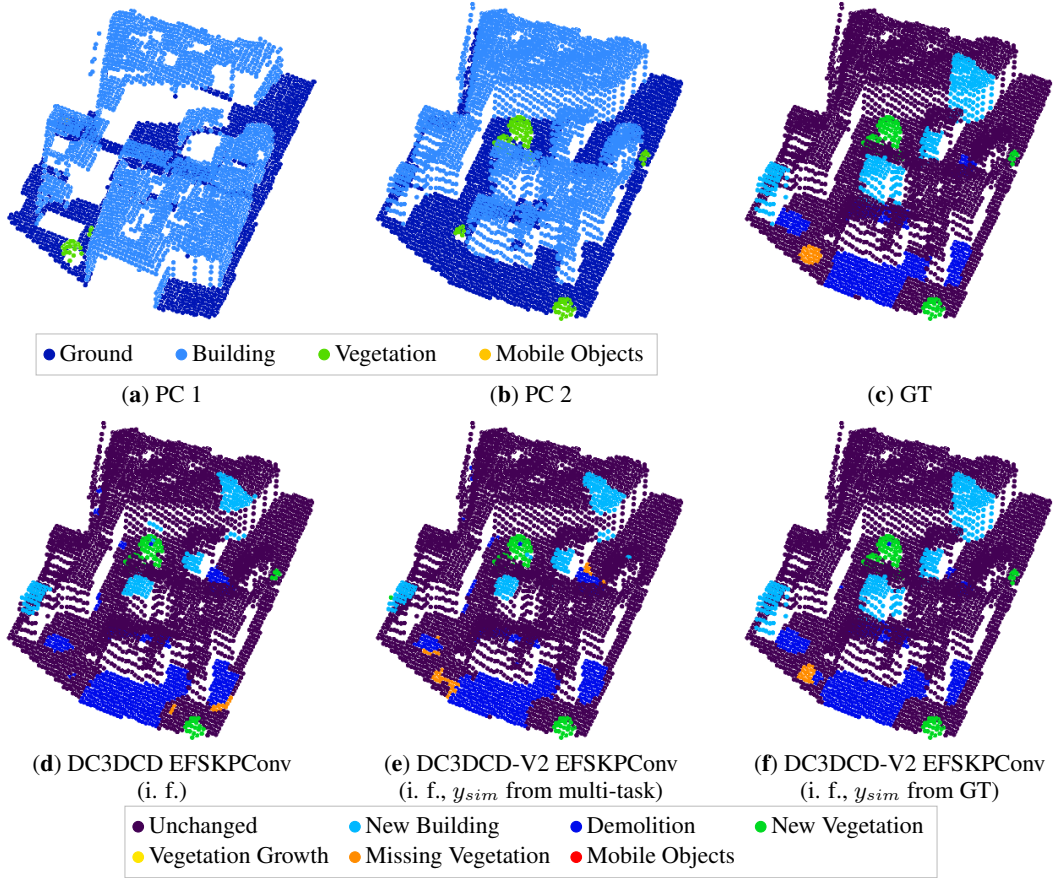


Figure 11: **Visual change detection results on Urb3DCD-V2 low density LiDAR sub-dataset:** (a-b) the two input point clouds; (c) ground truth (GT): simulated changes; (d) DC3DCD with the *Encoder Fusion SiamKPCnv* architecture and 10 hand-crafted input features (i. f.) results; (e) DC3DCD-V2 with the *Encoder Fusion SiamKPCnv* architecture, 10 hand-crafted input features results and the similarity y_{sim} computed from the multi-task configuration ($K_{mono-date} = 500$); (f) DC3DCD-V2 with the *Encoder Fusion SiamKPCnv* architecture, 10 hand-crafted input features results and the similarity y_{sim} computed from the ground truth (GT).

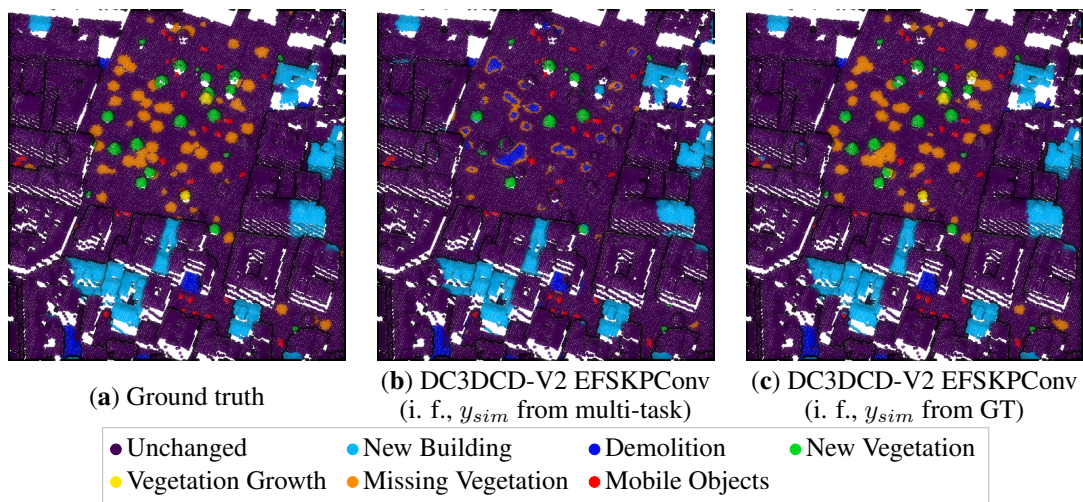


Figure 12: **Visual change detection results on Urb3DCD-V2 low density LiDAR sub-dataset (area 2):** (a) ground truth (GT): simulated changes; (b) DC3DCD-V2 with the *Encoder Fusion SiamKPCnv* architecture, 10 hand-crafted input features (i. f.) and the similarity y_{sim} computed from the multi-task configuration ($K_{mono-date} = 500$); (c) DC3DCD-V2 with the *Encoder Fusion SiamKPCnv* architecture, 10 hand-crafted input features and the similarity y_{sim} computed from the ground truth (GT). For comparison, one can refer to Figure 7 providing k -means and DC3DCD results over the same area.